Chapter 8
MODELING OF PORE FLUID DEPENDENT BEHAVIOR IN CHALK

INTRODUCTION

Pore fluid composition has been known for many years to greatly affect the mechanical behavior of high-porosity chalk. The stiffness, pore collapse yield strength, shear strength, tensile strength, and creep rate have all been shown to be affected by the pore fluid, as described in Chapter 3. The strength of water-saturated English outcrop chalk in unconfined compression was reported by Meigh and Early (1957) to be 2 to 3 times less than that of corresponding air-dry or oven-dry chalk. Numerous experimental studies performed in the intervening years have confirmed that dry chalks are stronger than oil-saturated chalks, which are in turn stronger than water-saturated chalks (see Carter and Mallard, 1974; Newman, 1983; Matthews and Clayton, 1993; Risnes et al., 1994; Schroeder and Shao, 1996; Risnes et al., 1996; Papamichos et al., 1997; Risnes and Flaageng, 1999; Gutierrez et al., 2000; Homand and Shao, 2000; Talesnick et al., 2001; Collin et al., 2002; Risnes et al., 2003; Risnes et al., 2004; and PASACHALK, 2004).

In the laboratory, the pore fluid composition *immediately* affects the mechanical behavior of North Sea chalks and outcrop chalks. A common laboratory test program which reveals this behavior is the "water injection" test in which a chalk, initially oil-saturated or nearly so, becomes water-saturated or nearly so when water is continuously injected from one end of the sample and displaces the oil in a piston-like manner. Water injection tests show consistently that compaction magnitude and rate increase immediately after water injection (Newman, 1983; Huegas and Charlez, 1990; Andersen et al., 1992; Vanggaard and Christensen, 1994; Schroeder and Shao, 1996; Papamichos et al., 1997; Schroeder et al., 1998; Homand and Shao, 2000; JCR database). In fact, local strain-gage measurements made during water injection tests (Schroeder et al., 1998; Homand and Shao, 2000) indicate that the increase in compaction and rate of compaction occurs immediately, at the position of the advancing waterfront where water displaces oil, rather than uniformly throughout the compacting sample; see Chapter 3 for typical results. The laboratory-scale water injection test results mimic the field-scale petroleum recovery operations, in which the water saturation of the entire field increases continuously due to petroleum extraction and water injection. Using and understanding the laboratory test results is therefore very important in predicting and controlling reservoir behavior. Because the

displacement of air or oil by water in chalk causes an immediate decrease in strength, the phenomenon has been termed “water weakening.”

MECHANISMS OF WATER WEAKENING

Several causal mechanisms of water weakening, including both chemical and physical mechanisms, have been proposed. The proposed chemical processes include: pressure solution, in which solid material undergoes dissolution in areas of high stress concentration and precipitates in areas with lesser stress concentrations; the stress-corrosion effect, in which changes in pore fluid composition decrease the stress threshold at which micro-cracks form within mineral crystals; and the Rebinder effect (Rebinder and Likhtman, 1957), in which the pore fluid affects the surface properties of the solid grains, which in turn affects the inter-granular behavior of the chalk. Pressure solution has been shown to occur in chalks (Hellmann et al., 1996), while stress corrosion has been observed in sandstone reservoir rocks (Hadizadeh and Law, 1991). It should be noted that these two chemical mechanisms of water weakening require significant passage of time to occur. Using chemical mechanisms to explain water weakening, it is assumed that chalk behavior varies as a function of pore fluid composition because the constitutive parameters which govern chalk behavior vary as a function of pore fluid composition.

The physical mechanism of capillarity and suction has also been proposed as the water weakening mechanism for chalks containing multi-phase pore fluids. Suction is the pressure difference between the non-wetting fluid and wetting fluid (*i.e.*, water) in the chalk. Suction does not develop in the presence of a single-phase pore fluid. The basis for the suction mechanism is that under conditions of low water saturation, the water menisci bind more tightly to the preferentially water-wet solids as water saturation decreases; this action causes suction and effective inter-granular stress to increase as water saturation decreases (Figure 8.1), which in turn increases the apparent cohesion or attraction in the chalk. The Barcelona Basic Model (Alonso et al., 1990), which is based on the suction mechanism and the theory of unsaturated soil mechanics, has been incorporated into the constitutive models of Papamichos et al. (1997), Collin et al. (2002), and DeGennaro et al. (2003) for chalk. Another physical property (fluid viscosity) was also investigated (Schroeder and Shao, 1996) but concluded to be insignificant to water weakening. Using the suction mechanisms to explain water weakening, it is assumed that chalk

behavior varies as a function of pore fluid composition because the effective stresses which govern chalk behavior vary as a function of pore fluid composition.

Most recently, Risnes et al. (2003, 2004) have shown that the variability of chalk strength with water activity, for pore fluids with both inorganic (*i.e.*, chloride salts) and organic (*i.e.*, glycol) solutes, is nearly identical to the variability of chalk strength with oil content. The mechanism which accounts for water weakening due to changes in water activity is probably a physical-chemical mechanism, but the specific mechanism of water weakening due to water activity is unknown.

Although capillary suction and effective stress changes has been implemented, using the Barcelona Basic Model, in several constitutive models as the mechanism that causes water weakening, this mechanism is believed to be inadequate to account for all observed effects of water-weakening. Several lines of evidence support this assumption. First, Lord et al. (1998) performed thermal decomposition-mass spectrometry analyses on reservoir chalks and found that dry chalks do not contain sufficient adsorbed water to support capillary water menisci and activate the suction mechanism. However, laboratory studies of partially water-saturated chalks (Schroeder and Shao, 1996; Collin et al., 2002; DeGennaro et al., 2003; PASACHALK, 2004) invalidate this conclusion and show that partially saturated chalks do develop capillary suction at low water contents (Figure 8.1). It seems reasonable to conclude that capillary suction is present in chalks saturated with multiphase pore fluids. Second, Risnes et al. (2003, 2004) have shown that chalk saturated with fully miscible water-glycol solutions is much stronger than water-saturated chalk. Since both water and water-glycol solutions are homogeneous single-phase fluids, no suction or change in effective stress develops in chalk samples saturated with either of these fluids; yet the mechanical behavior is different. Therefore, the behavioral difference cannot be due to differences in suction and effective stress. Third, the observed yield strength differences between oil-saturated chalks and water-saturated chalks under hydrostatic compression conditions are too great to be attributed to changes in suction alone (Gutierrez and Hickman, 2003). Fourth, the observed change in shear strength with pore fluid composition manifests itself by a change both in cohesion (or attraction) and in failure shear stress ratio, as observed consistently in published shear strength data (Risnes et al., 1996; Papamichos et al., 1997; Homand and Shao, 2000; Collin et al., 2002). In all of the experimental programs referenced, the failure shear stress ratio was greater for oil-saturated chalk than for water-

saturated chalk. Since the inter-granular friction angle is a property of the solid surfaces, the experimental data again supports the conclusion that some mechanism other than suction alone (*e.g.*, the Rebinder effect) is responsible for water weakening. If water weakening was due only to change in suction and effective stress, the same failure shear stress ratio should result from any pore fluid composition. Fifth, the Barcelona Basic Model does not account for the observed change in creep rate and other rate-dependent behavior associated with changes in pore fluid composition. It has been observed in many laboratory tests that creep rate varies significantly with different pore fluids (Schroeder and Shao, 1996; PASACHALK, 2004; JCR database), which cannot be explained by suction and effective stress changes alone.

The specific mechanisms which cause changes in mechanical behavior of chalk with different pore fluid compositions are therefore unknown. The variability of chalk behavior as a function of pore fluid which is incorporated into the constitutive model is based on observed behavior. Because the model is based on observed behavior, it is not possible to quantitatively predict the changes in mechanical behavior as a function of pore fluid composition from first physical principles alone.

PROPOSED CHALK MODEL AND PORE FLUID DEPENDENCE

The proposed constitutive model for chalk is described in detail in Chapter 6. The model incorporates rate-dependence with an elliptical viscoplastic potential surface, a shear failure surface, and a tensile failure surface. The model requires 12 parameters to fully describe the rate-dependent behavior of chalk. Of the 12 parameters, seven vary regularly as a function of pore fluid composition: (1) bulk modulus K; (2) reference time-line anchor N; (3) attraction a; (4) adjusted failure shear stress ratio $\overline{\eta}_f$; (5) cap aspect ratio M; (6) creep parameter ψ; and (7) tensile strength p_t. Two other parameters (Poisson's ratio ν, compression coefficient λ) vary irregularly with pore fluid composition.

Qualitatively, the effect that pore fluid composition has on each of these parameters is easily determined from inspection of lab test results. As water saturation increases, the parameters change as follows: (1) K decreases; (2) N decreases; (3) a decreases; (4) $\overline{\eta}_f$ decreases; (5) M decreases; (6) ψ increases; and (7) p_t decreases. However, determining the quantitative nature of variation of each of these parameters with pore fluid composition is difficult, due to the small number of tests performed with different pore fluids, the many

different pore fluid combinations that have been tested, the inherent variability of chalk composition and behavior with even a single pore fluid, and the other factors (*e.g.*, porosity) that influence chalk behavior. An attempt to quantify the pore fluid dependence of these parameters follows in the next section.

PARAMETER VALUES FOR CHANGED PORE FLUID COMPOSITION

Correlations between model parameter values and pore fluid composition are introduced in this section. As mentioned above, these correlations are based on only a few data points and should therefore be used with caution. Many of the relationships presented in the literature are presented in the context of one of the proposed causal mechanisms of water weakening: Papamichos et al. (1997) present parameter values as a function of water saturation, Collin et al. (2002) and DeGennaro et al. (2003) present parameter values as a function of suction, and Risnes et al. (2003, 2004) present parameter values as a function of water activity.

Bulk modulus K decreases as water saturation increases, as determined from hydrostatic compression tests on water-saturated chalks. The correlation between bulk modulus and porosity for oil-saturated chalks is given in Chapter 6. A similar correlation between bulk modulus and porosity for water- or brine-saturated chalks is shown in Figure 8.2. For water- and brine-saturated chalks:

$$K(\text{in MPa}) = 84000 \exp(-11.3n) \tag{8.1}$$

The data of Figure 8.2(b) shows that while some overlap between the two groups exists, the bulk modulus for water- and brine-saturated chalks is consistently less than that for oil- and gas-saturated chalks. The observed bulk modulus decreases continuously as water content increases (Papamichos et al., 1997) or as water activity increases (Risnes et al., 2004). Data from Papamichos et al. (1997) indicates that most of the variability in the bulk modulus-water saturation relationship in partially saturated chalks occurs at low water saturations, while the data of Risnes et al. (2004) suggests that the change in bulk modulus with water activity in water-glycol saturated chalks is more gradual (Figure 8.3).

The observed preconsolidation stress p_c is much less in water-saturated chalk than in oil-saturated chalk (Papamichos et al., 1997; Schroeder et al., 1998; Homand and Shao, 2000; Talesnick et al., 2001; Risnes, 2001; Collin et al., 2002; DeGennaro et al., 2003; Risnes et al.,

2003). For water-saturated chalks, the best-fit relationship between porosity and apparent preconsolidation stress as determined from hydrostatic compression tests is (Figure 8.4a):

$$p_c\,(\text{in MPa}) = 350\exp(-7.7n) \tag{8.2}$$

This relationship is significantly different from the corresponding relationship for oil-saturated chalks. As shown in Figure 8.4b, some overlap between the oil-saturated and water-saturated chalk data sets exists. However, the effect of pore fluid composition and water weakening on apparent preconsolidation stress is clear: water-saturated chalks are weaker in pore collapse than are oil-saturated chalks.

As discussed later, it is assumed that the compression coefficient λ varies with porosity identically for all pore fluid compositions. As for oil-saturated chalks, equations (8.2) and (6.21) may be substituted into equation (6.17) to obtain a relationship between the reference time-line anchor N and porosity n for water-saturated chalks:

$$N = \frac{n}{1-n} + (0.141 - 0.185n)\exp(4.5n) \tag{8.3}$$

The variability of values for attraction a, adjusted failure shear stress ratio $\overline{\eta}_f$, and cap aspect ratio M with pore fluid composition is largely unknown due to the small number of data sets available for comparison with different pore fluids. The best data sets available for comparison are summarized in Table 8.1. For all five data sets, the adjusted failure shear stress ratio is greater for oil-saturated chalks (or equivalent) than for water-saturated chalks; the ratio $\overline{\eta}_f$ (oil)/ $\overline{\eta}_f$ (water) ranges from 1.05 to 1.37, with an average value of 1.15. For four of the five data sets, the attraction is greater for oil-saturated chalks (or equivalent) than for water-saturated chalks. The ratio a(oil)/a(water) ranges from 0.6 to 2.0, with an average value of 1.36. In the absence of field-specific data, the use of these multipliers for these parameters is recommended.

It is assumed that the adjusted failure shear stress ratio $\overline{\eta}_f$ and cap aspect ratio M vary coincidentally such that $M \approx \overline{\eta}_f$. Therefore, it is recommended to use the same multiplier for M as for $\overline{\eta}_f$.

For waterflooding tests, values for creep parameter ψ exist for the same chalk sample under both oil-saturated and water-saturated conditions. The values of ψ for both oil-saturated conditions and water-saturated conditions are shown in Table 8.2. For these tests, the ratio

ψ(oil)/ ψ(water) ranges from 1.08 to 1.63, with an average value of 1.41. Additional data from the PASACHALK project is used to obtain a ratio between oil-saturated and water-saturated conditions. The constant-rate of strain data shown in Figure 5.16 is reproduced in Figure 8.5. As discussed in Chapter 5, the slope of the best-fit line in log-log space is proportional to the value of the creep multiplier. For the data of Figure 8.5, the ratio ψ(oil)/ ψ(water) equals 1.70. In addition, the value ψ(air)/ ψ(oil) equals 1.77. In the absence of field-specific data, the use of these multipliers for the creep parameter is recommended.

Little data exists to determine correlations of tensile strength p_t to porosity for water-saturated chalks. The data of Risnes et al. (2004) for water-glycol mixtures indicates that the value of p_t (oil)/ p_t (water) is approximately 2.3.

It is interesting that no published laboratory data exists regarding the mechanical behavior of multiphase oil-water saturated chalks in shear failure and tensile failure, and that the data of Schroeder et al. (1998) is the only published data with respect to the mechanical behavior of multiphase oil-water saturated chalks in pore collapse. The mechanical behavior of chalk saturated with intermediate oil-water mixtures was observed by Schroeder et al. to make a transition from "oil-like" behavior to "water-like" behavior at small values (about 2.5 %) of water saturation. The data for partially saturated chalks (Papamichos et al., 1997) closely resembles the data of Schroeder et al. for multiphase oil-water saturated chalks. For example, the preconsolidation stress p_c varies with water saturation in a very similar way for partially saturated chalks and multiphase oil-water saturated chalks (Figure 8.6). Figure 8.6a shows the raw data for these samples, while Figure 8.6b shows the data normalized to the oil-saturated strength. The data trends of Papamichos et al. for partially saturated chalks will be extrapolated here for use with multiphase oil-water saturated chalks. A general best-fit equation for the data of Figure 8.6b is:

$$p_c = p_{c,\min} + \left(p_{c,\max} - p_{c,\min}\right)\left(1 - S_w\right)^b \tag{8.4}$$

In equation (8.4), $p_{c,\text{relative}}$ is the preconsolidation stress relative to the maximum value (*i.e.*, for oil-saturated chalk), $p_{c,\min}$ is the minimum preconsolidation stress (*i.e.*, for water-saturated chalk), S_w is the water saturation, and b is a fitting parameter. For the data of Figure 8.6b, $p_{c,\min} = 0.5$ and $b = 30$.

The variability of unconfined compressive strength with water saturation (Papamichos et al., 1997) fits exactly the same trend as the preconsolidation stress data (Figure 8.7). It will be assumed, then, that all parameters which are affected by water weakening can be described by the same general form of equation (8.4):

$$x = x_{\min} + (x_{\max} - x_{\min})(1 - S_w)^b \tag{8.5}$$

In equation (8.5), x can stand for any of the parameters that vary as a function of pore fluid composition: these include bulk modulus K, reference time-line anchor N, attraction a, adjusted failure shear stress ratio $\overline{\eta}_f$, cap aspect ratio M, creep parameter ψ, and tensile strength p_t. A value for $x_{\min}$ for each parameter may be obtained from the data given in this chapter, or from laboratory data, while it is recommended to use a value of 20 to 30 for the exponent b.

Poisson's ratio ν does not vary regularly with pore fluid composition. Several K_0 compression tests from the JCR database on chalks saturated with multiphase brine-oil fluids in different proportions show a general independence of Poisson's ratio with respect to pore fluid composition. It is notable that while the values for Poisson's ratio in the JCR database range from 0.20 to 0.27 for oil-saturated chalks as stated in Chapter 6, several chalks saturated with multiphase fluids and greater water saturations exhibit lesser values of Poisson's ratio, although the variation is not regular (Figure 8.8a). Papamichos et al. (1997), Homand and Shao (2000), and DeGennaro et al. (2003) used the same values for Poisson's ratio for oil-saturated and water-saturated chalks because capillary suction and change in effective stress is believed to be the water-weakening mechanism in their models. Collin et al. (2002) use a greater value of Poisson's ratio for water-saturated chalk than for oil-saturated chalk. Risnes et al. (2004) obtained values of Poisson's ratio which range from 0.11 to 0.25 for chalk saturated with water-glycol solutions (Figure 8.8b). The data of Risnes et al. suggests that Poisson's ratio increases with increasing water activity or water saturation, which is exactly the opposite conclusion suggested by the data from the JCR database. The most rational conclusion which may be drawn from the data is that the effects of pore fluid composition on Poisson's ratio are uncertain, both qualitatively and quantitatively. It appears to be reasonable to use the same values of Poisson's ratio for both multiphase-saturated chalk and oil-saturated chalk.

As observed in hydrostatic compression tests on water-saturated chalks, the compression coefficient λ is greater for water-saturated chalk than for oil-saturated chalk. The best-fit

relationship between porosity and compression coefficient for water-saturated chalks is (Figure 8.9):

$$\lambda = 0.052 \exp(3.5n) \tag{8.6}$$

The best-fit relationship is quite different from the corresponding relationship for oil-saturated chalks, and indicates that water-saturated chalks are more compressible than oil-saturated chalks. However, this relationship is deceiving for the following two reasons: (1) All the laboratory test data used to form this relationship for water-saturated chalks was obtained using global displacement and strain measurements, which is known to be greater than local strain-gage measurements (Hayano et al., 2001). For the tests in which data was collected using both local and global measurements, a greater value of λ was obtained using global measurements; the difference in λ ranges from 5 to 68 % and averages 20 %. In contrast, the data used to form the relationship shown in Chapter 6 for oil-saturated chalks was obtained using local measurements. Therefore, at least part of the apparent increased compressibility of water-saturated chalks is due to measurement error; (2) In waterflooding tests, the value of λ generally decreases between the test stage in which the chalk is oil-saturated and the stage in which the chalk is water-saturated. Table 8.3 shows that in 3 of 5 waterflooding tests, $\lambda_{oil} \geq \lambda_{water}$; this trend is opposite that indicated by comparing equations (6.21) and (8.6). It is concluded, then, that the effect of pore fluid composition of the value of λ is irregular. It is recommended to use the same value of λ for all pore fluids unless laboratory data that indicates otherwise is available.

MODEL BEHAVIOR DUE TO CHANGE IN PORE FLUID COMPOSITION

Simulation of mechanical behavior of chalk for the case in which the pore fluid composition remains constant throughout loading is described in Chapters 5 and 6. The rate-dependent model for chalk behavior is described by linear elasticity with an elliptical cap viscoplastic potential surface, a shear failure surface, and a tensile failure surface. Values for the 12 required model parameters may be obtained from laboratory test results, or may be obtained using the correlations with porosity given in Chapter 6 (for oil-saturated chalk) or in Chapter 8 (for water-saturated chalk or multiphase fluid-saturated chalk). In the case of constant pore fluid composition, the elliptical cap expands in stress space as the chalk is volumetrically compressed, while the shear and tensile failure surfaces are fixed in stress space throughout loading.

Changes in pore fluid composition cause the values of many model parameters to change. Three of these parameters (reference time-line anchor N, bulk modulus K, and creep parameter ψ) affect the behavior of the one-dimensional model; the other parameters (cap aspect ratio M, attraction a, adjusted failure shear stress ratio $\overline{\eta}_f$, and tensile strength p_t) affect the size and shape of the viscoplastic potential surface and shear and tensile failure surfaces in p-q space. When a change in pore fluid composition is simulated, it is important to use the parameter values that correspond to the proper pore fluid composition.

Changes in pore fluid composition cause complications in material behavior. The failure surfaces and viscoplastic potential surfaces are generally different for oil-saturated and water-saturated chalk. For a pore fluid composition which contains both oil and water, the values for the model parameters which govern chalk behavior lie between those which are applicable to oil- and water-saturated chalk. The appropriate values for the model parameters may be determined for a given pore fluid composition by interpolating between the corresponding surfaces for oil- and water-saturated chalks.

Recall from Chapter 5 that the one-dimensional rate-dependent model appears as a set of time-lines which are straight lines in e-log p space (Figure 5.1). The reference time-line is described by two parameters: the reference time-line anchor N and the compression coefficient λ. For a given chalk, the value for N when water-saturated is less than the value for N when oil-saturated (Figure 8.10). The value of N for an intermediate pore fluid composition is between N_{oil} and N_{water}. Although this condition is not true in general, Figure 8.10 assumes that λ has the same value for all pore fluids; therefore, $\lambda_{oil} = \lambda_{water}$. For rate-independent behavior, the reference time-line is the same as the yield surface.

For two identical chalk samples with different pore fluids (*i.e.*, oil and water) loaded in one-dimensional hydrostatic compression, chalk yields at a lesser mean stress when water-saturated than when oil-saturated. This behavior is shown schematically in Figure 8.11 for constant-rate compression tests. The behavior of Figure 8.11 is consistent with the test data shown in Figure 8.12 for two nearly identical samples of Tyra field chalk with different pore fluids. In each case, since the pore fluid composition is constant throughout each test, the appropriate reference time-line is unchanged throughout the duration of the test.

When the pore fluid composition changes during loading, however, the material behavior is not so simple. When the pore fluid changes from oil to water, as during a waterflooding test,

the gradual change in pore fluid changes the position of the reference time-line. If it is assumed that λ is constant for all pore fluid compositions, the value of N alone controls the position of the reference time-line. The value of N for a given pore fluid composition may be obtained using equation (8.5) where N is the variable of interest. N decreases as the water saturation increases in the pore fluid. Since the volumetric age and creep rate depend on the proximity of the stress point to the reference time-line in e-ln p space, the volumetric age of chalk under a constant stress state decreases as water saturation increases (Figure 8.13). Large inelastic strains may accumulate if the pore fluid composition changes sufficiently.

In three-dimensional loading conditions, shear failure, tensile failure, and non-hydrostatic pore collapse are possible. Several model parameters which affect the size and/or shapes of the viscoplastic potential surface and failure surfaces modes change their values as a result of water weakening: these parameters include the cap aspect ratio M, attraction a, adjusted failure shear stress ratio $\overline{\eta}_f$, and tensile strength p_t. The changes in the size and shape of the viscoplastic potential surface and shear and failure surfaces become effective immediately when pore fluid composition changes (Figure 8.14). For example, waterflooding of an oil-saturated chalk under shear failure conditions causes a significant change in stress due to the corresponding change in shear strength (Figure 8.15). A similar stress change may occur during waterflooding of an oil-saturated chalk under tensile failure conditions (Figure 8.16). Note in Figure 8.15 that the stress change $\Delta\sigma_{ij}$ due to waterflooding occurs in the direction of plastic flow.

COMPARISON WITH EXPERIMENTAL RESULTS

Many waterflooding tests have been performed in the laboratory, including both mechanical and creep loading stages, to determine the creep behavior of North Sea chalk with different pore fluids. The rate-dependent chalk model with provisions for pore fluid dependence was used to simulate several of these results for deep-sea and outcrop chalks as described in this section.

Six simulations illustrate the performance of the model during waterflooding tests under K_0 conditions. Two simulations apply to Stevns Klint outcrop chalk, three simulations apply to Tyra field chalk, and one simulation applies to Valhall field chalk. Multiple mechanical and creep loading stages were performed during all tests on Stevns Klint and Tyra chalk, while multiple mechanical and stress relaxation loading stages were performed during the test on

Valhall chalk. In each test, at least one creep and/or stress relaxation stage was performed on each oil-saturated and water-saturated chalk.

For the waterflooding test simulations on Stevns Klint outcrop chalk (Files 460 and 461), all required parameter values for bulk modulus K, cap aspect ratio M, eccentricity parameter R, and compression coefficient λ_{oil} for oil-saturated chalk were obtained using the correlations to porosity given in Chapter 6. The values for creep parameter ψ_{oil} and minimum volumetric age $t_{v,min}$ were obtained from laboratory data; the value for Poisson's ratio ν was obtained using the mean value for all oil-saturated chalks; and a value of attraction a = 1 MPa was assumed for the outcrop chalk.. These values are given in Table 8.4. The value for the reference time-line anchor N_{oil} was obtained by trial and error to best fit the test data. The corresponding parameter values for water-saturated Stevns Klint chalk were then obtained using the correlations and recommended values given in this chapter. The value for K_{water} was obtained using equation (8.1); the values for creep parameter ψ_{water}, minimum volumetric age $t_{v,min}$, reference time-line anchor N_{water}, and compression coefficient λ_{water} were obtained from laboratory data; and other parameter values were obtained as follows:

$$M_{water} = M_{oil} / 1.15 \tag{8.9}$$

$$R_{water} = R_{oil} \tag{8.10}$$

$$\nu_{water} = \nu_{oil} \tag{8.11}$$

$$a_{water} = a_{oil} / 2 \tag{8.12}$$

The parameter values for water-saturated chalk are also given in Table 8.4.

The results from the waterflooding test simulations on Stenvs Klint outcrop chalk are shown in Figures 8.17 and 8.18. In all figures, the point at which water injection was performed is indicated. The simulated creep behavior, stress-strain behavior, and stress path all closely match the observed behavior. Therefore, the model seems to have the capability to closely simulate the effects of waterflooding in Stevns Klint chalk.

For the waterflooding simulations on Tyra field chalk, the values for parameters K, M, R, and λ for oil-saturated chalk were all obtained using the correlations from Chapter 6. The values for ψ_{oil} and $t_{v,min}$ were obtained from laboratory test data; the value of ν was obtained using the mean value for all oil-saturated chalks; and a value of a = 4 MPa was assumed for deep-sea chalk.

The values for N_{oil} and N_{water} were obtained to match the data of Files 453 and 452 for oil- and water-saturated chalk, respectively. The corresponding values of K, M, R, ν, and a for water-saturated Tyra chalk were obtained using equations (8.1) and (8.9)-(8.12), while the values for ψ_{water}, $t_{v,min}$, N_{water}, and λ_{water} were obtained from laboratory test data. All parameter values for the waterflooding tests on Tyra chalk are shown in Table 8.5.

The results on the single-fluid K_0 compression tests on Tyra field chalk are shown in Figures 8.19 and 8.20. The results from the waterflooding test simulations on Tyra chalk are shown in Figures 8.21 to 8.23. In all figures, the point at which water injection was performed is indicated. The simulated creep behavior, stress-strain behavior, and stress path all closely match the observed behavior. Therefore, the model seems to have the capability to closely simulate the effects of different pore fluids and waterflooding in Tyra chalk.

For the waterflooding simulation on Valhall field chalk, the values for parameters K, M, R, and λ for oil-saturated chalk were all obtained using appropriate values from Chapter 6 for a representative porosity value for Valhall chalk. The values for ψ_{oil}, ψ_{water}, and $t_{v,min}$ were obtained by trial and error, although the ratio between ψ_{oil} and ψ_{water} was obtained from laboratory test data; the value of ν was obtained using the mean value for all oil-saturated chalks; and a value of a = 4 MPa was assumed for deep-sea chalk. For this simulation, it was assumed that $K_{oil} = K_{water}$, on the basis of observed laboratory data. The corresponding values of M, R, ν, and a for water-saturated Valhall chalk were obtained using equations (8.9)-(8.12). All parameter values for the waterflooding test on Valhall chalk are shown in Table 8.6.

The results from the waterflooding test simulation on Valhall chalk are shown in Figure 8.24. In the figures, the point at which water injection was performed is indicated. The simulated stress relaxation behavior, stress-strain behavior, and stress path all closely match the observed behavior. Therefore, the model seems to have the capability to closely simulate the effects of different pore fluids and waterflooding in Valhall chalk.

DISCUSSION ON THE WATERFLOODING MODEL

The way that pore fluid effects are incorporated into the constitutive model for chalk are different from any other model proposed previously. In addition to changing only the creep parameter or only changing the rate-independent elastoplastic parameters to account for changes in pore fluid composition, this formulation changes both to account for changes in shape of the

yield and viscoplastic potential surface and for changes in time-dependent behavior. Using this formulation, the values for all required model parameters can be obtained from laboratory tests, and the model is able to closely simulate observed chalk behavior under all tested conditions with different pore fluids, using only the values from the laboratory tests.

REFERENCES

Alonso, E.E., Gens, A., and Josa, A. (1990). A constitutive model for partially saturated soils. Geotechnique, 40(3), 405-430.

Andersen, M.A., Foged, N., and Pedersen, H.F. (1992). The link between waterflood-induced compaction and rate-sensitive behaviour in weak North Sea chalk. Proceedings of the 4th North Sea Chalk Symposium, Deauville, France, 15 p.

Carter, P.G. and Mallard, D.J. (1974). A study on the strength, compressibility, and density trends within the chalk of southeast England. Quarterly Journal of Engineering Geology, 7, 43-55.

Collin, F., Cui, Y.J., Schroeder, C., and Charlier, R. (2002). Mechanical behavior of Lixhe chalk partly saturated by oil and water: experiment and modeling. International Journal for Numerical and Analytical Methods in Geomechanics, 26, 897-924.

Datcheva, M., Charlier, R., and Collin, F. (2001). Constitutive equations and numerical modeling of time effects in soft porous rocks. Lecture Notes in Computer Science, 1988, 222-229.

DeGennaro, V., Delage, P., Cui, Y.-J., Schroeder, C., and Collin, F. (2003). Time-dependent behaviour of oil reservoir chalk: a multiphase approach. Soils and Foundations, 43(4), 131-147.

Gutierrez, M. and Hickman, R.J. (2003). Modeling of soft rock-fluid interaction as acceleration of time-dependent behavior. Presentation given at 16th ASCE Engineering Mechanics Conference, Seattle.

Gutierrez, M., Oino, L.E., and Hoeg, K. (2000). The effect of fluid content on the mechanical behavior of fractures in chalk. Rock Mechanics and Rock Engineering, 22(2), 93-117.

Hadizadeh, J. and Law, R.D. (1991). Water-weakening in sandstone and quartzite deformed at various stress and strain rates. International Journal of Rock Mechanics and Mining Sciences and Geomechanics Abstracts, 28(5), 431-439.

Hayano, K., Matsumoto, M., Tatsuoka, F., and Koseki, J. (2001). Evaluation of time-dependent properties of sedimentary soft rock and their constitutive modeling. *Soils and Foundations*, 41 (2), 21-38.

Hellmann, R., Gratier, J.P., and Renders, P. (1996). Deformation of chalk by pressure solution. Proceedings of V.M. Goldschmidt Conference, Heidelberg, Germany.

Homand, S., and Shao, J.F. (2000). Mechanical behavior of a porous chalk and effect of saturating fluid. Mechanics of Cohesive-Frictional Materials, 5, 583-606.

Huegas, O. and Charlez, P. (1990). Mechanical effect of water injection of Ekofisk chalk. Proceedings of 3rd North Sea Chalk Symposium, Copenhagen.

Lord, C.J., Johlman, C.L., and Rhett, D.W. (1998). Is capillary suction a viable cohesive mechanism in chalk? Proceedings of EUROCK '98, Trondheim, Norway, 1, 479-486.

Matthews, M.C. and Clayton, C.R.I. (1993). Influence of intact porosity on the engineering properties of a weak rock. In: Proceedings of Geotechnical Engineering of Hard Soils-Soft Rocks (Anagnostopoulos et al., eds.), 693-702.

Meigh, A.C. and Early, K.R. (1957). Some physical and engineering properties of chalk. Proceedings of 4th International Conference on Soil Mechanics and Foundation Engineering, 68-73.

Newman, G.H. (1983). The effect of water chemistry on the laboratory compression and permeability characteristics of some North Sea chalks. Journal of Petroleum Technology, 35(5), 976-980.

Papamichos, E., Brignoli, M., and Santarelli, F.J. (1997). An experimental and theoretical study of a partially saturated collapsible rock. Mechanics of Cohesive-Frictional Materials, 2, 251-278.

PASACHALK (2004). Mechanical Behavior of Partially and Multiphase Saturated Chalks Fluid-Skeleton Interaction: Main Factor of Chalk Oil Reservoirs Compaction and Related Subsidence – Part 2, Final Report, EC Contract no. ENK6-2000-00089.

Rebinder, P.A. and Likhtman, V. (1957). Effect of surface-active media on strain and rupture in soils. Proceedings of 2nd International Conference on Surface Activity, 563-580.

Risnes, R. (2001). Deformation and yield in high porosity outcrop chalk. Physics and Chemistry of the Earth (A), 26(1-2), 53-57.

Risnes, R. and Flaageng, O.F. (1999). Mechanical properties of chalk with emphasis on chalk-fluid interactions and micromechanical aspects. Oil and Gas Science and Technology, 54(6) 751-758.

Risnes, R., Gjesdal, S.A., Landaas, T.L., and Madland, I. (1994). Changes in mechanical properties of chalk caused by deformation and by pore pressure. Proceedings of EUROCK '94, Delft, The Netherlands, 853-860.

Risnes, R., Haghighi, H., Korsnes, R.I., and Natvik, O. (2003). Chalk-fluid interactions with glycol and brines. Tectonophysics, 370, 213-226.

Risnes, R., Hole, M., and Kwabiah, N.K. (2004). Chalk-fluid interactions with water-glycol mixtures. Proceedings of Workshop on Chalk Mechanical Behavior, Stavanger, Norway, Feb. 3-4, 33 p.

Risnes, R., Kristensen, C.N., and Andersen, M.A. (1996). Triaxial tests on high porosity chalk with different saturating fluids. Proceedings of the 5th North Sea Chalk Symposium, Riems, France, 12 p.

Schroeder, C. and Shao, J.F. (1996). Plastic deformation and capillary effects in chalks. Proceedings of the 5th North Sea Chalk Symposium, Reims, France, 14 p.

Schroeder, C., Bois, A.-P., Maury, V., and Halle, G. (1998). Water/chalk (or collapsible soil) interaction: part II. Results of tests performed in laboratory on Lixhe chalk to calibrate water/chalk models. Proceedings of EUROCK '98, Trondheim, Norway, 505-514.

Talesnick, M.L., Hatzor, Y.H., and Tsesarsky, M. (2001). The elastic deformability and strength of a high porosity, anisotropic chalk. International Journal of Rock Mechanics and Mining Sciences, 38, 543-555.

Vanggaard, M. and Christensen, H.F. (1994). Waterflooding of oil-saturated Stevns outcrop chalk. Proccedings of EUROCK '94, Delft, The Netherlands, 845-852.

Table 8.1. Comparison of shear strength data for oil- and water-saturated chalks.

Reference	Oil-saturated		Water-saturated	
	Adjusted failure shear stress ratio $\overline{\eta}_f$	Attraction a	Adjusted failure shear stress ratio $\overline{\eta}_f$	Attraction a
Collin et al. (2002); PASACHALK (2004)	1.23	2.6 MPa	1.03	1.7 MPa
Homand and Shao (2000)	0.68	3.0 MPa	0.65	1.5 MPa
Risnes and Flaageng (1998)	1.64*	0.8 MPa*	1.20	0.7 MPa
Papamichos et al. (1997)	1.16**	11.8 MPa**	1.09	7.3 MPa
Risnes and Kristensen (1996)	1.36	0.4 MPa	1.27	0.7 MPa

* methanol-saturated
** unsaturated

Table 8.2. Values of the creep parameter ψ for chalks under oil- and water-saturated conditions.

Test	ψ_{oil}	ψ_{water}
File 454	0.0032	0.0052
File 455	0.0041	0.0061
File 456	0.0025	0.0038
File 460	0.0052	0.0056
File 461	0.0054	0.0073

Table 8.3. Values of the compression coefficient λ for chalks under oil- and water-saturated conditions.

Test	λ_{oil}	λ_{water}
File 454	0.132	0.167
File 455	0.064	0.064
File 456	0.098	0.202
File 460	0.280	0.129
File 461	0.296	0.108

Table 8.4. Values for the model parameters for waterflooding simulations on Stevens Klint outcrop chalk.

Parameter	File 460		File 461	
	Oil	Water	Oil	Water
Bulk modulus K (MPa)	1300	550	1500	660
Poisson's ratio ν	0.24	0.24	0.24	0.24
Reference time-line anchor N	1.16	1.12	1.11	1.05
Compression coefficient λ	0.18	0.16	0.165	0.14
Cap aspect ratio M	0.96	0.84	1.02	0.89
Eccentricity parameter R	0.71	0.71	0.67	0.67
Attraction a (MPa)	1	0.5	1	0.5
Creep parameter ψ	0.0052	0.0056	0.0052	0.0071
Minimum volumetric age $t_{v,\min}$ (hours)	2	2	1.5	3

Table 8.5. Values for the model parameters for waterflooding simulations on Tyra field chalk.

Parameter	File 452	File 453	File 454	
	Water	Oil	Oil	Water
Bulk modulus K (MPa)	520	1250	1900	840
Poisson's ratio ν	0.24	0.24	0.24	0.24
Reference time-line anchor N	1.18	1.32	1.125	1.17
Compression coefficient λ	0.18	0.18	0.15	0.16
Cap aspect ratio M	0.82	0.94	1.11	0.97
Eccentricity parameter R	0.73	0.73	0.63	0.63
Attraction a (MPa)	2	4	4	2
Creep parameter ψ	0.0014	0.0014	0.0032	0.0052
Minimum volumetric age $t_{v,\min}$ (hours)	0.2	0.1	0.5	0.8
Parameter	File 455		File 456	
	Oil	Water	Oil	Water
Bulk modulus K (MPa)	1700	760	1400	580
Poisson's ratio ν	0.24	0.24	0.24	0.24
Reference time-line anchor N	0.98	1.17	1.025	1.28
Compression coefficient λ	0.10	0.16	0.10	0.19
Cap aspect ratio M	1.08	0.94	0.98	0.85
Eccentricity parameter R	0.64	0.64	0.70	0.70
Attraction a (MPa)	4	2	4	2
Creep parameter ψ	0.0041	0.0061	0.0025	0.0038
Minimum volumetric age $t_{v,\min}$ (hours)	0.4	0.4	0.2	0.3

Table 8.6. Values for the model parameters for waterflooding simulation on Valhall field chalk.

Parameter	File 500	
	Oil	Water
Bulk modulus K (MPa)	2100	2100
Poisson's ratio ν	0.24	0.24
Reference time-line anchor N	1.09	0.92
Compression coefficient λ	0.14	0.14
Cap aspect ratio M	1.17	1.02
Eccentricity parameter R	0.60	0.60
Attraction a (MPa)	4	2
Creep parameter ψ	0.0100	0.0145
Minimum volumetric age $t_{v,\min}$ (hours)	1	3

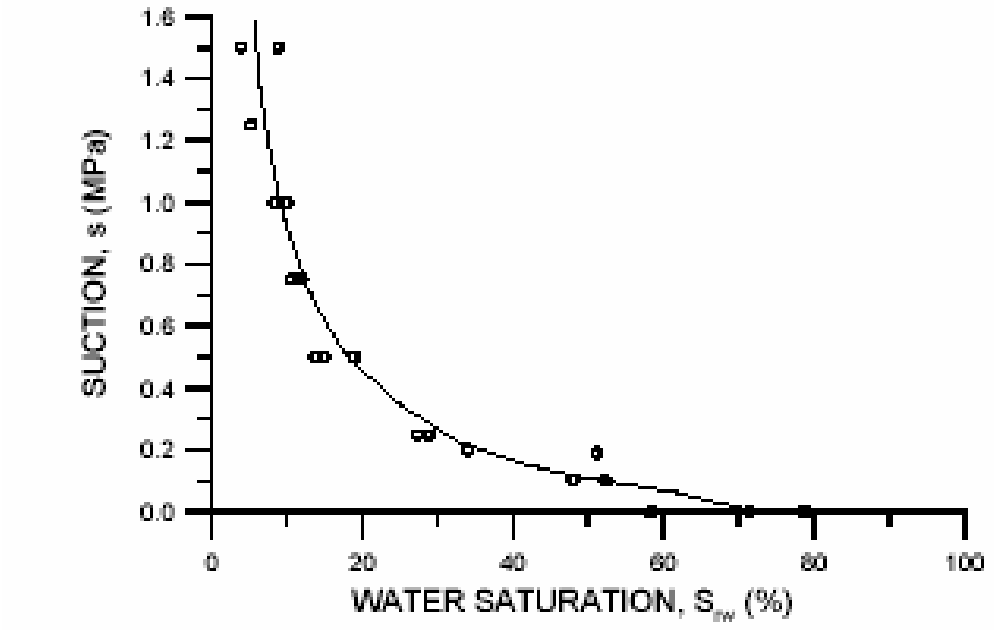

Figure 8.1. Suction, defined as the difference in pressures between the nonwetting fluid and the wetting fluid, increases as water content decreases for partially saturated Lixhe chalk (PASACHALK, 2004).

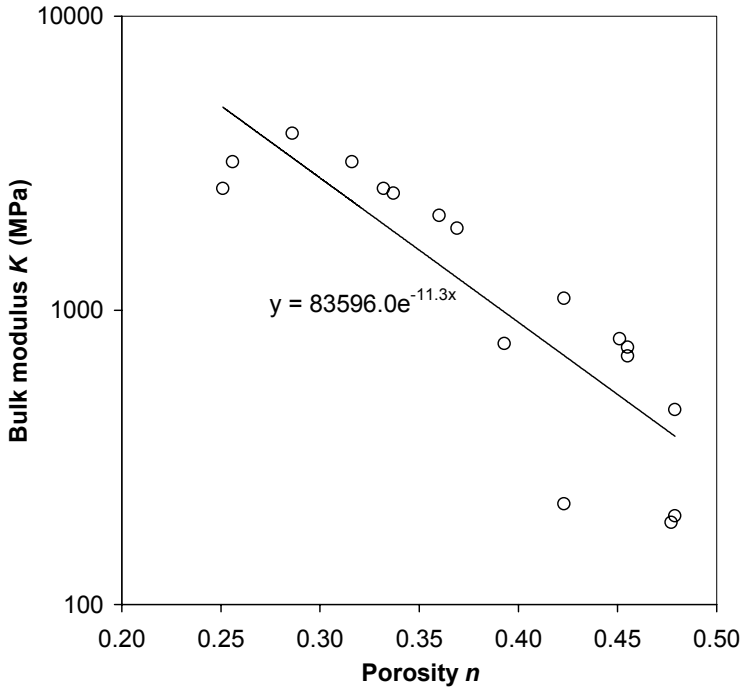

(a)

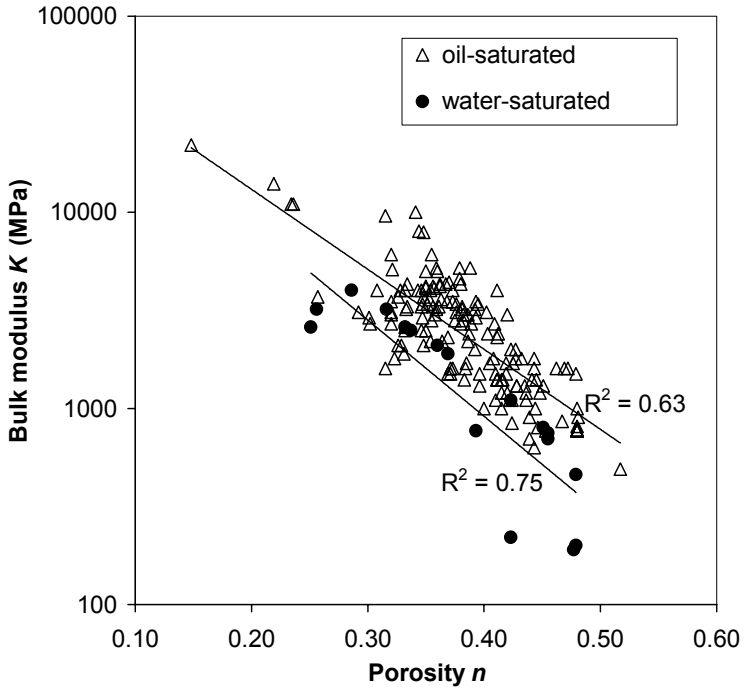

(b)

Figure 8.2. Correlation between porosity *n* and bulk modulus *K* (a) for water- and brine-saturated chalks only; (b) for oil-saturated chalks and water- or brine-saturated chalks. While some overlap between the two groups exists, the bulk modulus for water- and brine-saturated chalks is consistently less than that for oil-saturated chalks.

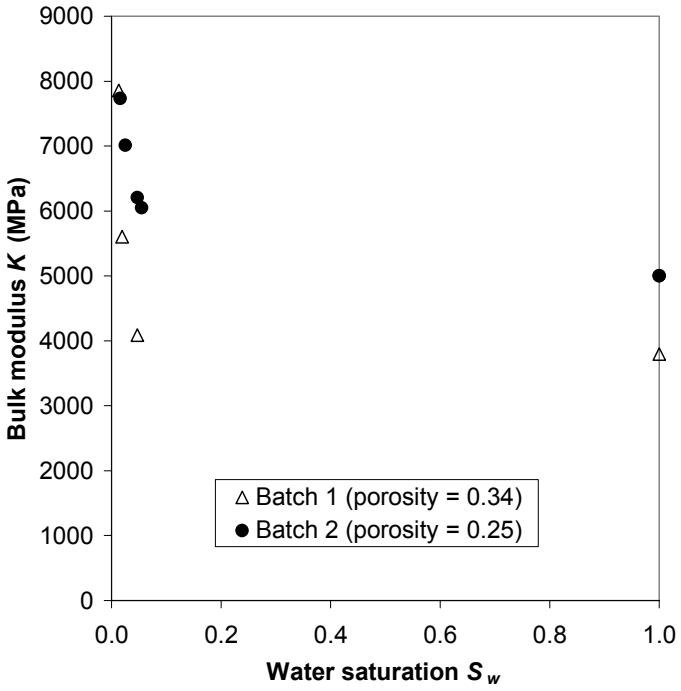

(a)

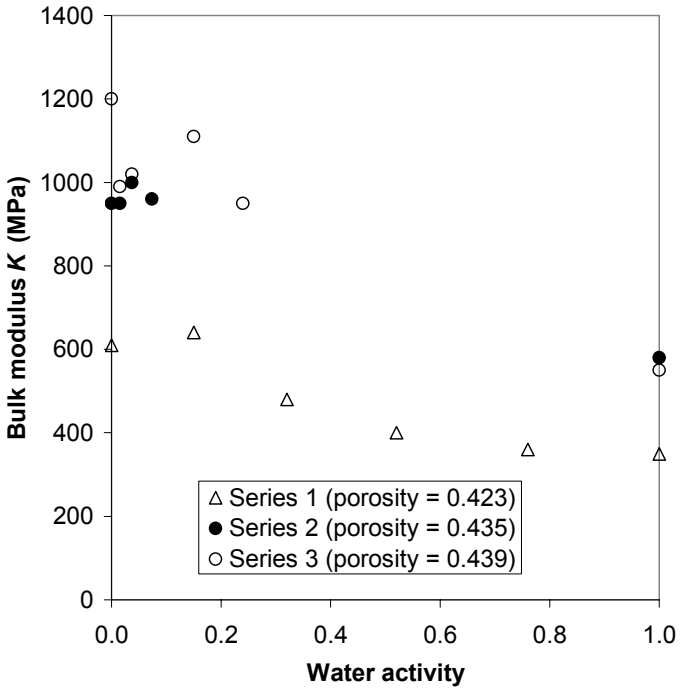

(b)

Figure 8.3. Variation in bulk modulus indicates that (a) for partially saturated chalks, the variability with water saturation is most pronounced at low water saturations (data for Pietra Lecesse chalk; after Papamichos et al., 1997); (b) for water-glycol saturated chalks, the variability with water activity is relatively uniform (after Risnes et al., 2004).

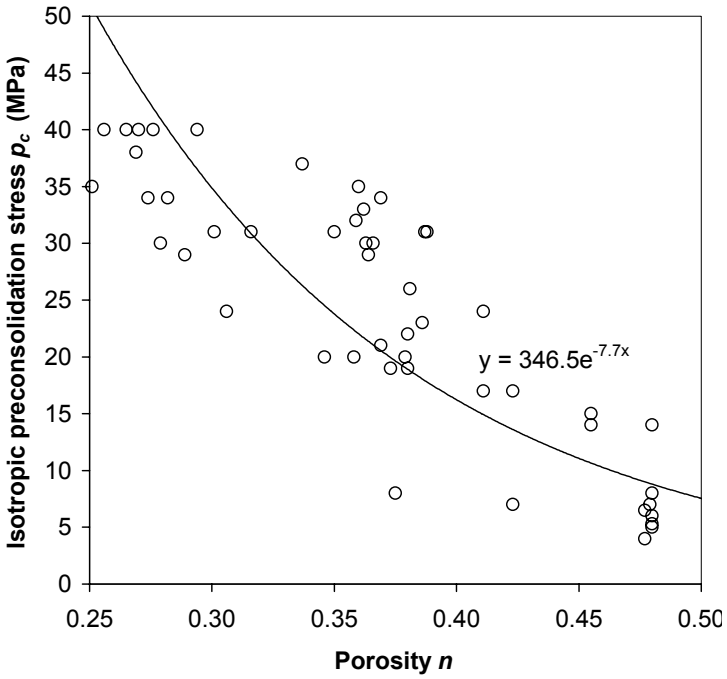

(a)

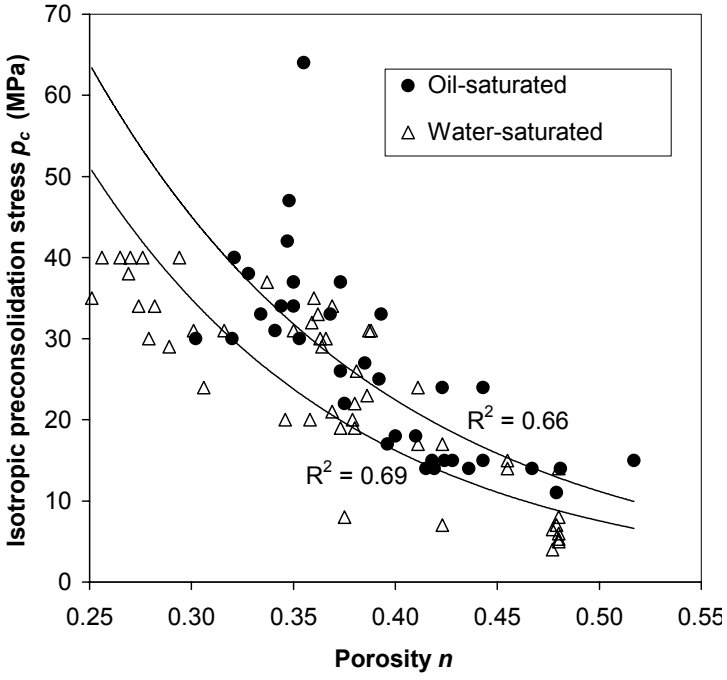

(b)

Figure 8.4. Correlation between porosity n and preconsolidation stress p_c (a) for water-saturated chalks only; (b) for oil-saturated chalks and water-saturated chalks. While some overlap between the two groups exists, the preconsolidation stress for water-saturated chalks is consistently less than that for oil-saturated chalks.

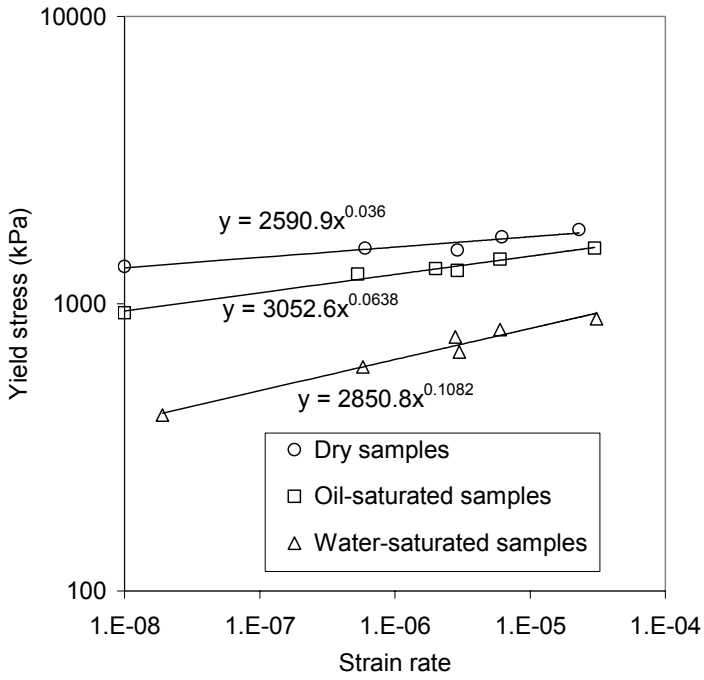

Figure 8.5. The slope of the best-fit line to strain rate-yield stress data in log-log space for constant-rate-of-strain tests is proportional to the creep parameter ψ. Use of many test results from Lixhe chalk saturated with various fluids indicates that $\psi_{air} > \psi_{oil} > \psi_{water}$ (after PASACHALK, 2004).

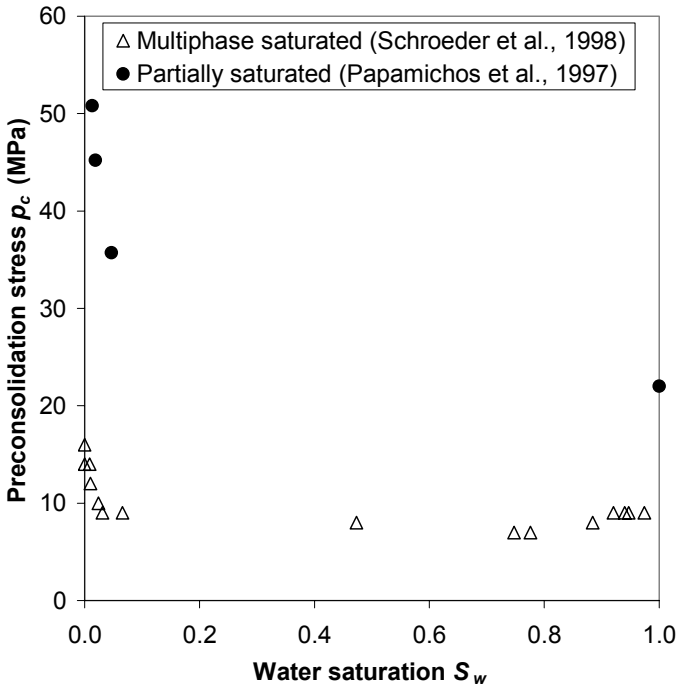

(a)

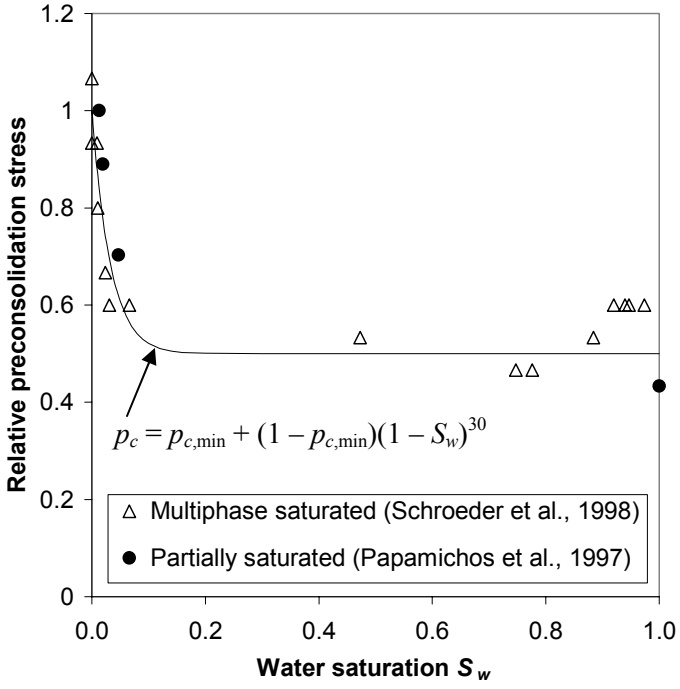

(b)

Figure 8.6. The variation of preconsolidation stress p_c with water saturation is very similar for partially saturated chalks and multiphase oil-water saturated chalks. The relationship in (a) shows the raw data, while (b) shows the data normalized to the value for oil-saturated chalk (after Papamichos et al., 1997, and Schroeder et al., 1998).

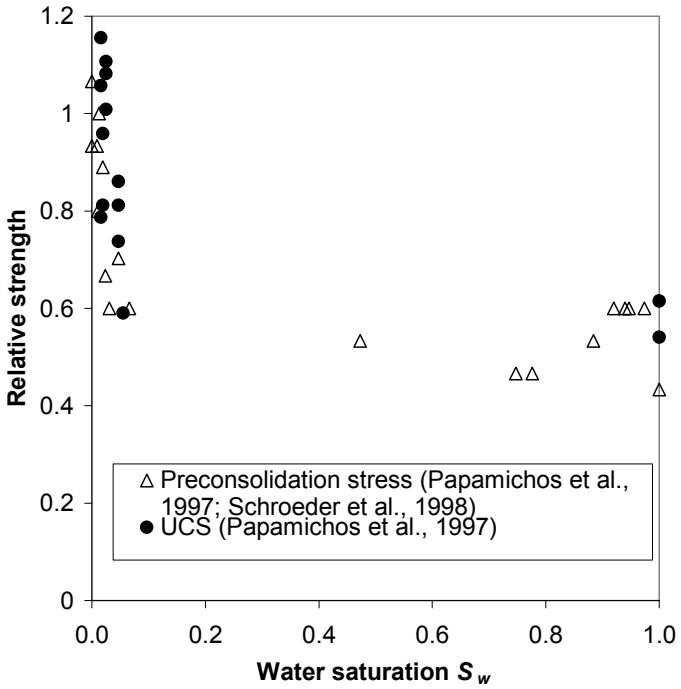

Figure 8.7. The variability of unconfined compressive strength with water saturation fits exactly the same trend as the preconsolidation stress data. Data from Papamichos et al. (1997); Schroeder et al. (1998).

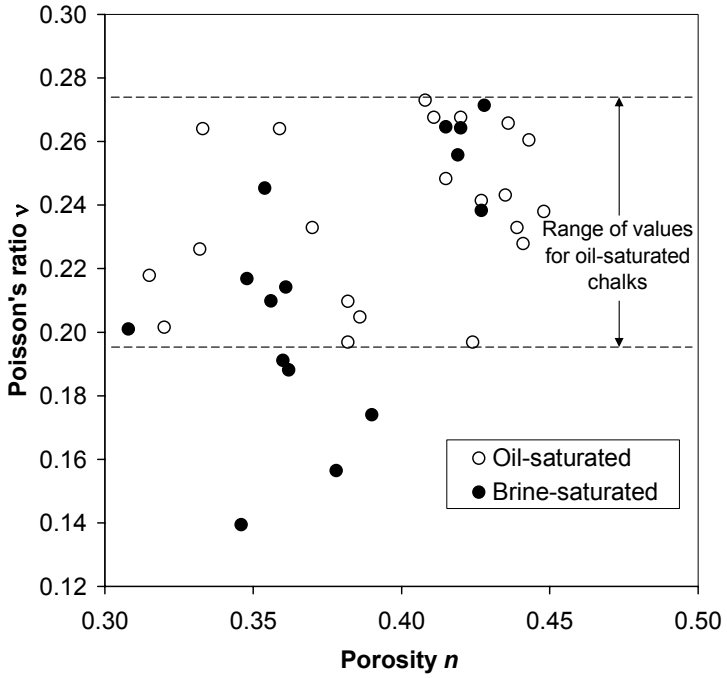

(a)

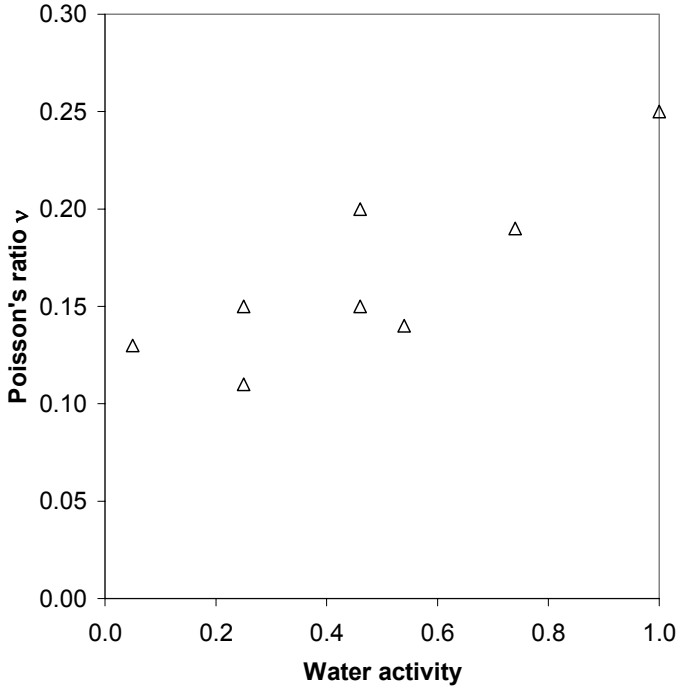

(b)

Figure 8.8. Dependency of Poisson's ratio on pore fluid composition is unclear: (a) range of values for Poisson's ratio in brine-saturated chalks includes lesser values than those for oil-saturated chalks (data from JCR database); (b) values for Poisson's ratio appear to increase as water activity increases in water-glycol mixtures (after Risnes et al., 2004).

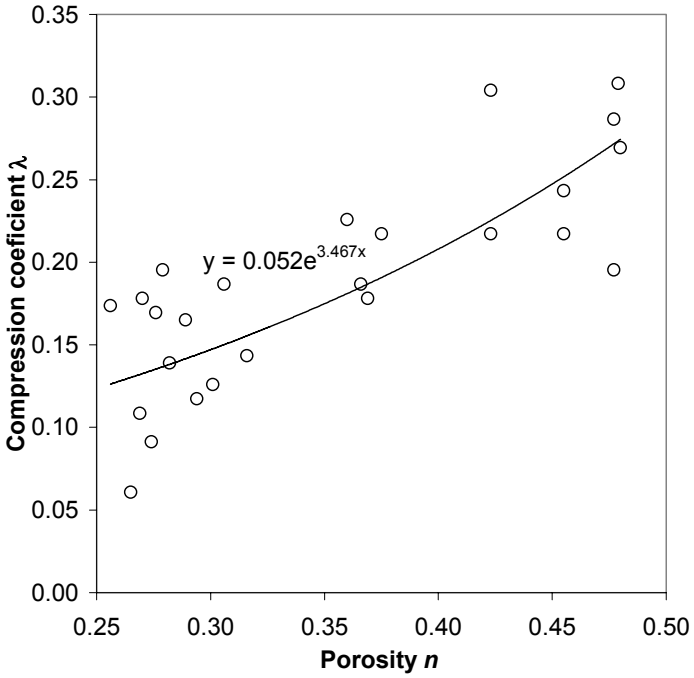

(a)

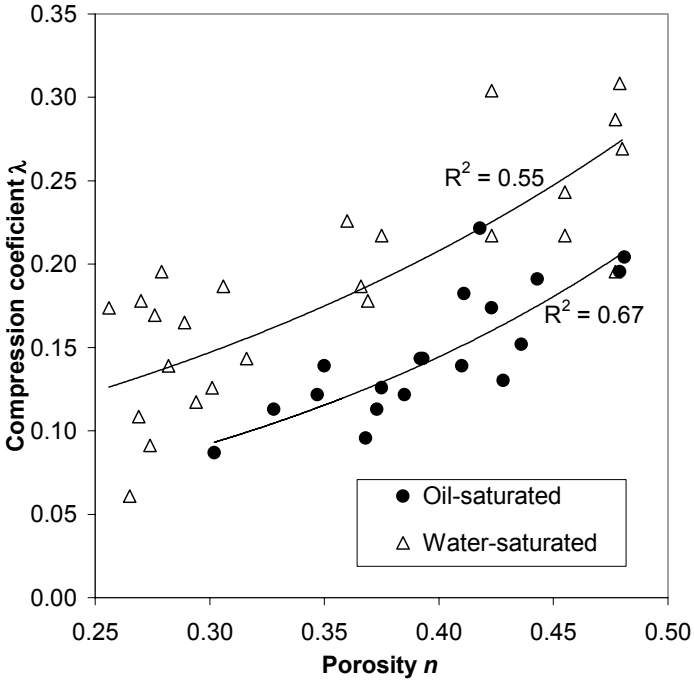

(b)

Figure 8.9. Correlation between porosity *n* and compression coefficient λ (a) for water-saturated chalks only; (b) for oil-saturated chalks and water-saturated chalks. While some overlap between the two groups exists, the compression coefficient for water-saturated chalks is consistently less than that for oil-saturated chalks.

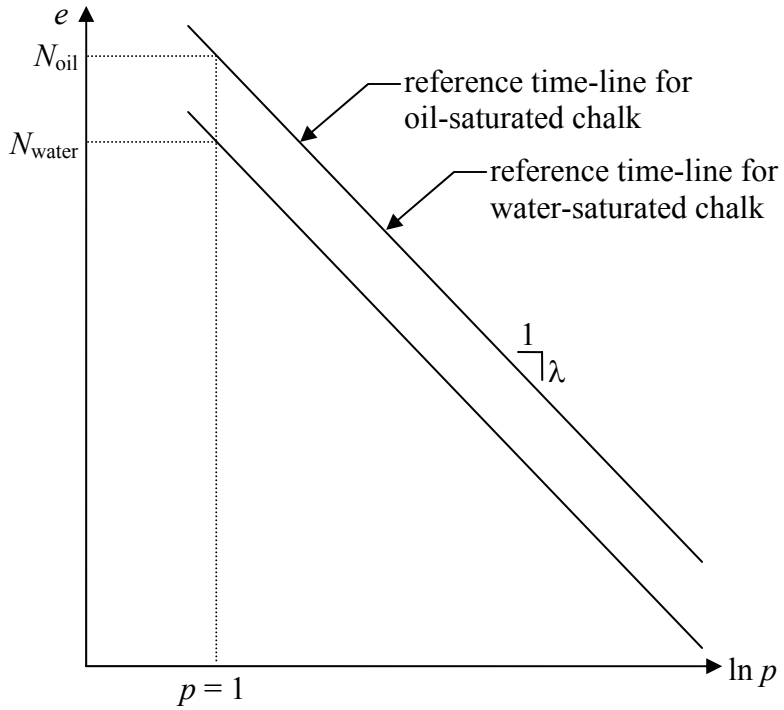

Figure 8.10. Original relative positions of the reference time-line anchors *N* for various pore fluids. For a given chalk, $N_{oil} > N_{water}$. This figure assumes that $\lambda_{oil} = \lambda_{water}$.

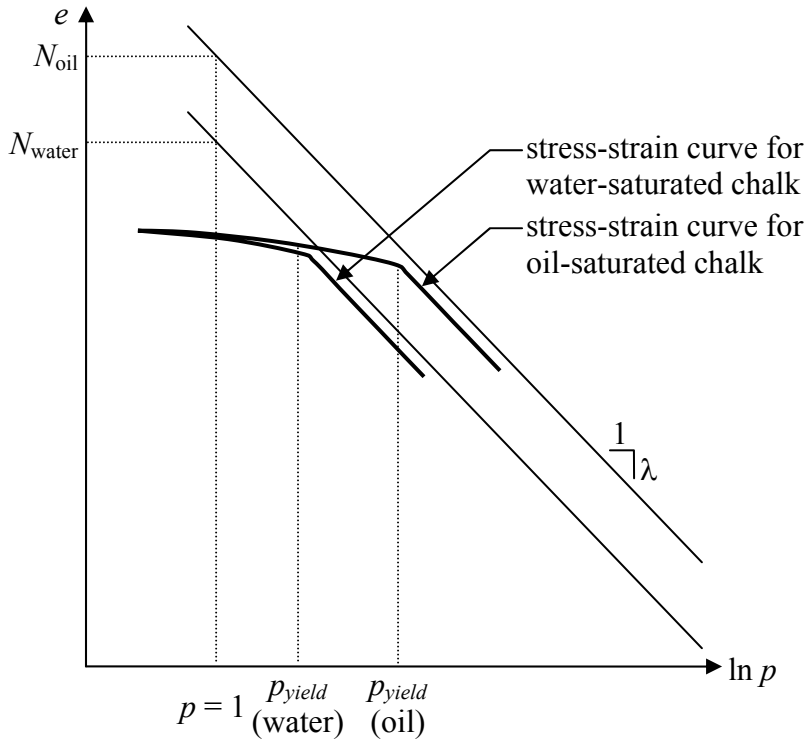

Figure 8.11. For identical chalk samples with different pore fluids loaded in hydrostatic compression, water-saturated chalk yields at a lesser mean stress than oil-saturated chalk.

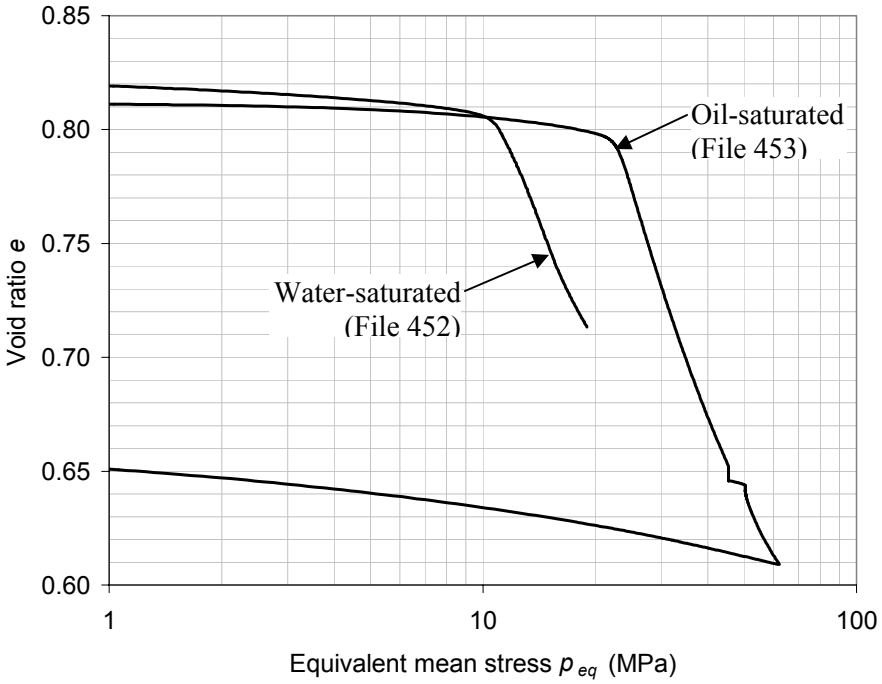

Figure 8.12. Data from Tyra field chalk (Files 452 and 453) illustrating behavior shown schematically in Figure 8.11.

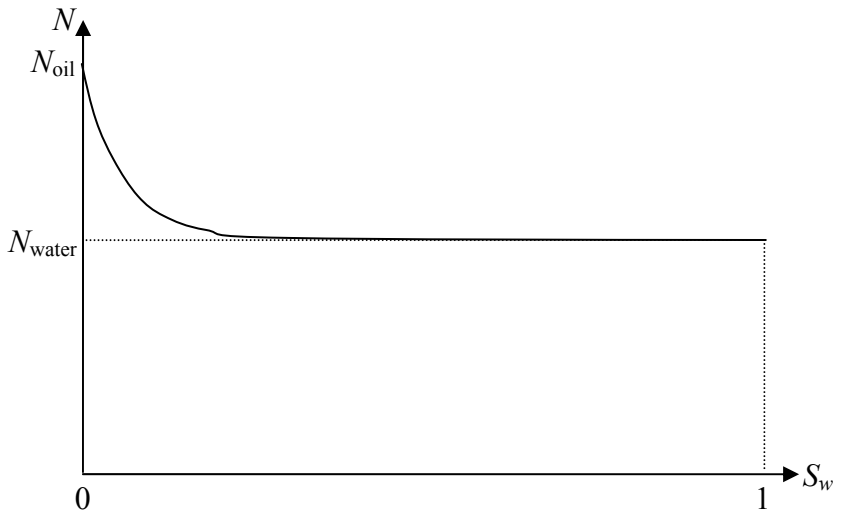

(a)

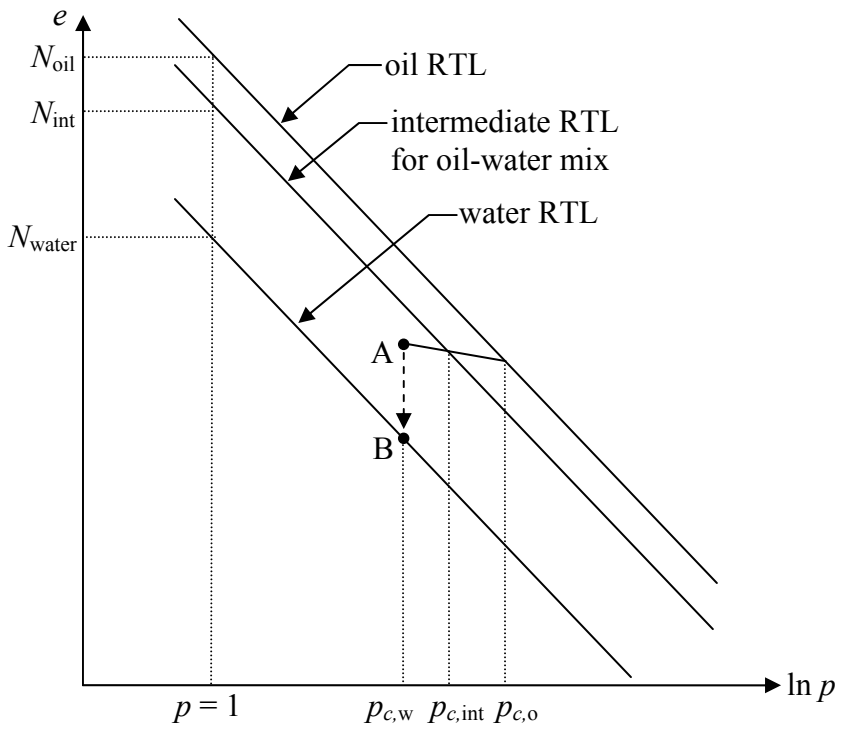

(b)

Figure 8.13. Volumetric age decreases and creep rate increases as water saturation increases under constant stress. In (a), the value of reference time-line (RTL) anchor N decreases as a smooth function of water saturation as in Figure 8.6(b). In (b), at the constant stress state of point A, the reference time-line anchor decreases from N_{oil} to N_{int} as the pore fluid changes from oil to an oil-water mixture, causing the preconsolidation stress to decrease from $p_{c,o}$ to $p_{c,int}$ and the volumetric age to decrease correspondingly. As the water saturation increases further to a full water-saturated state, the RTL anchor decreases to N_{water}, and large inelastic strains occur as the stress point moves from point A to point B.

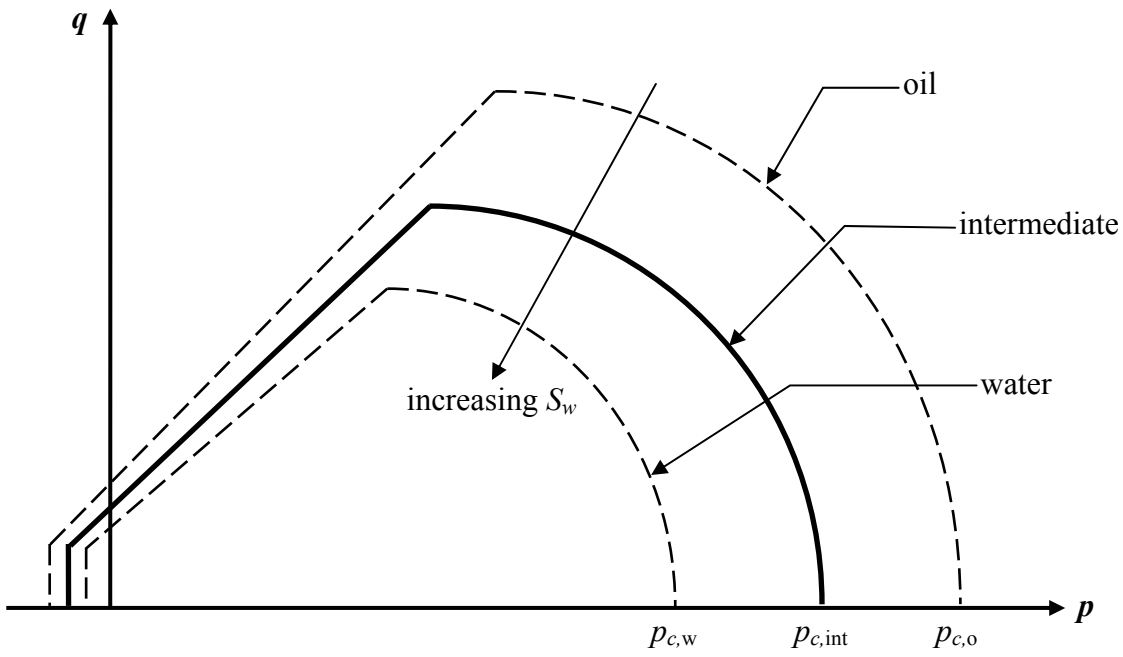

Figure 8.14. The size and shape of the yield surfaces and reference time-line changes instantly as the pore fluid composition changes. During waterflooding, the yield surfaces contract.

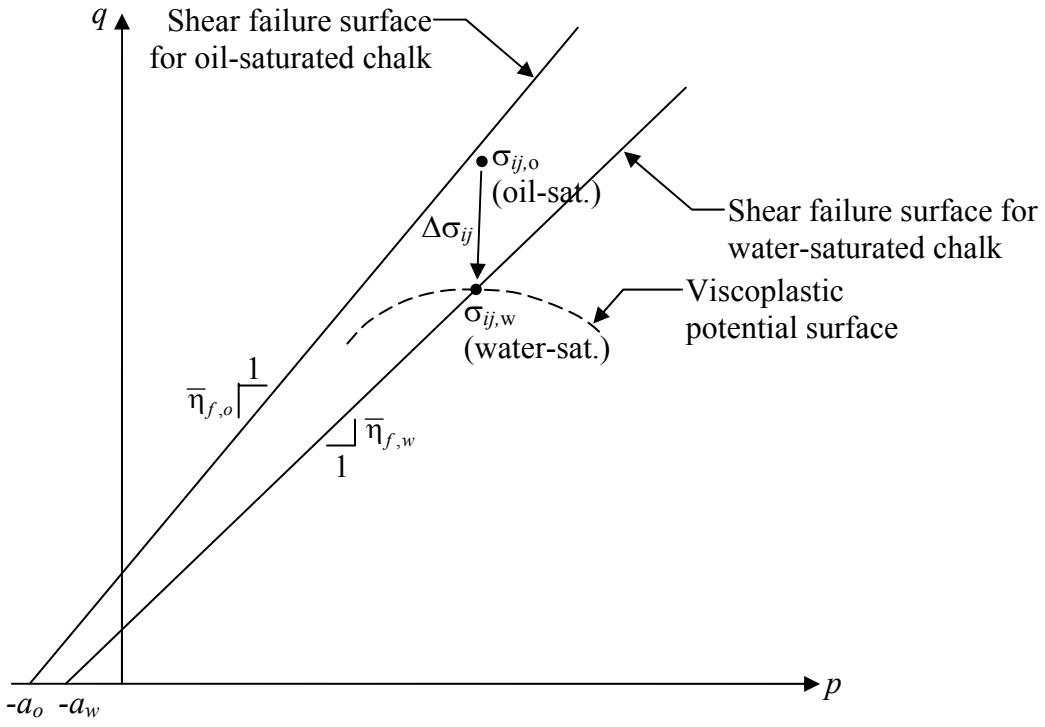

Figure 8.15. Waterflooding of an oil-saturated chalk under near-shear failure conditions causes a significant stress change $\Delta\sigma_{ij}$ due to the corresponding loss of shear strength. The subscripts *o* and *w* indicate oil-saturated and water-saturated conditions, respectively.

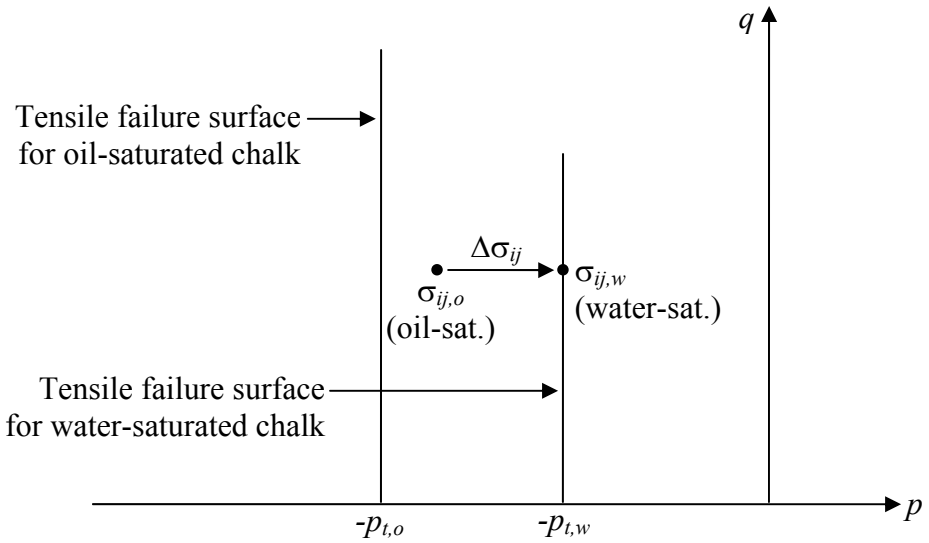

Figure 8.16. Waterflooding of an oil-saturated chalk under near-tensile failure conditions causes a stress change $\Delta\sigma_{ij}$ due to the corresponding loss of tensile strength. The subscripts *o* and *w* indicate oil-saturated and water-saturated conditions, respectively.

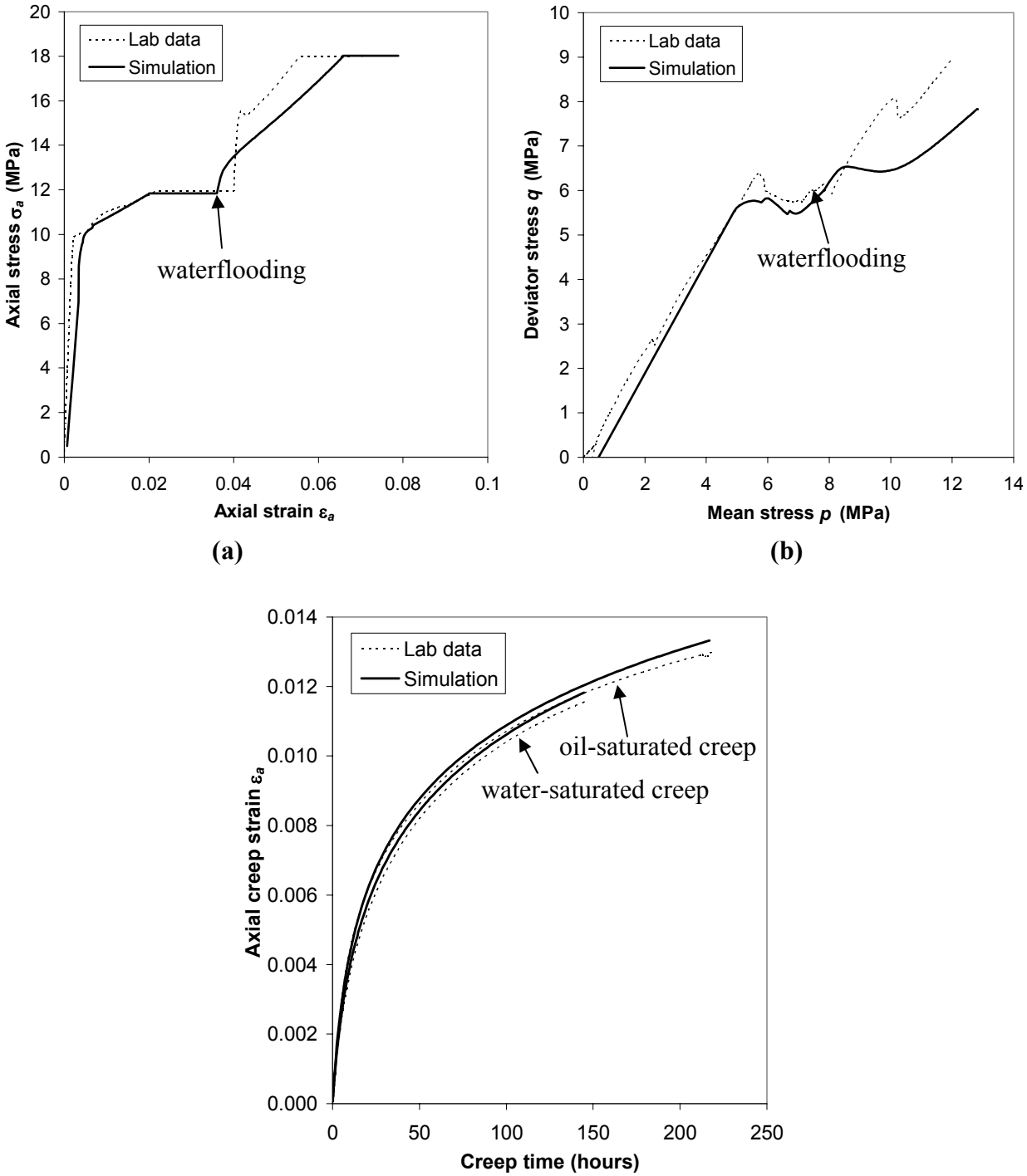

Figure 8.17. Results of simulated waterflooding test on Stevns Klint outcrop chalk (File 460). Results include (a) stress-strain curve; (b) stress path; and (c) creep curves.

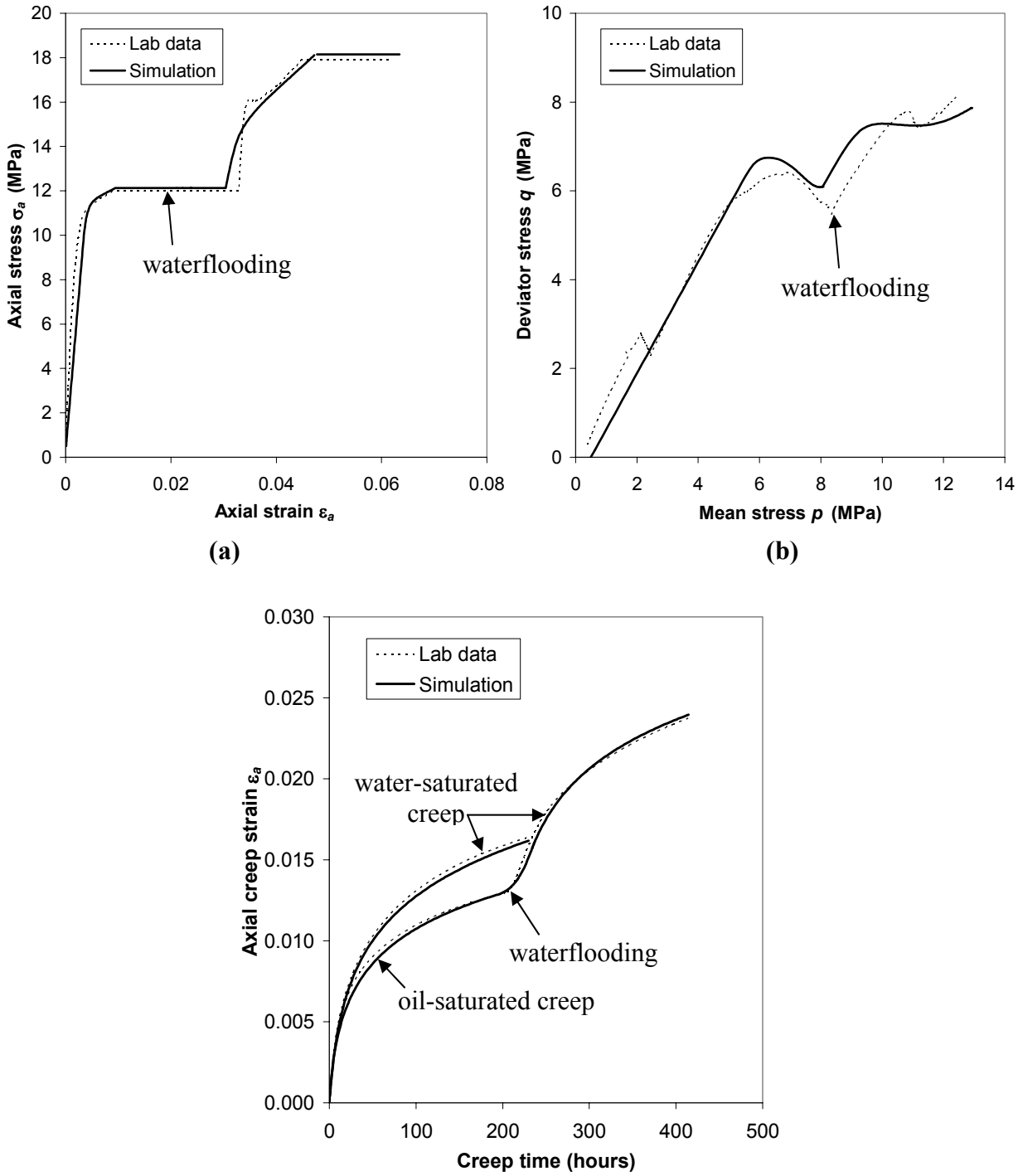

Figure 8.18. Results of simulated waterflooding test on Stevns Klint outcrop chalk (File 461). Results include (a) stress-strain curve; (b) stress path; and (c) creep curves.

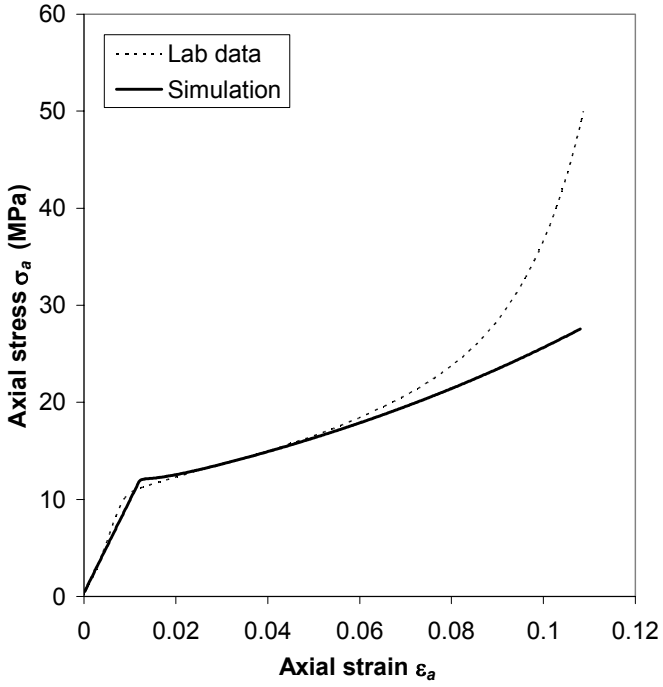

(a)

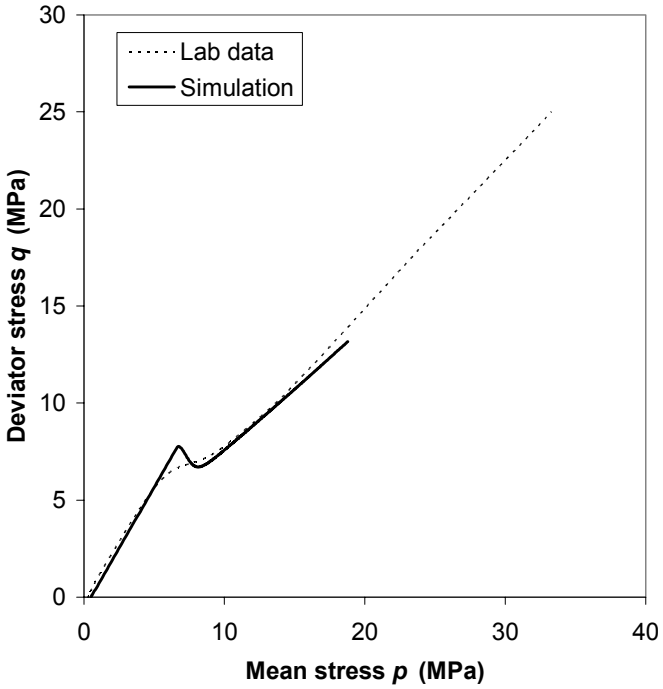

(b)

Figure 8.19. Results of simulated K_0 compression test on water-saturated Tyra field chalk (File 452). Results include (a) stress-strain curve; and (b) stress path.

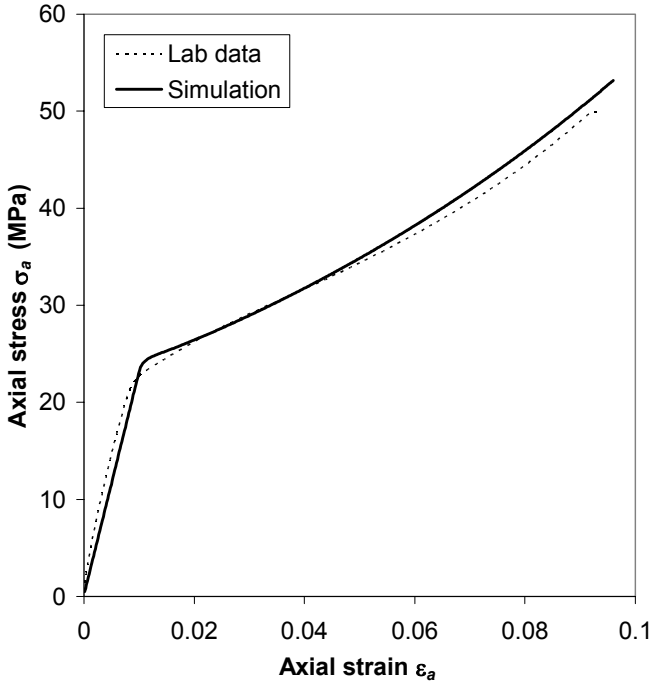

(a)

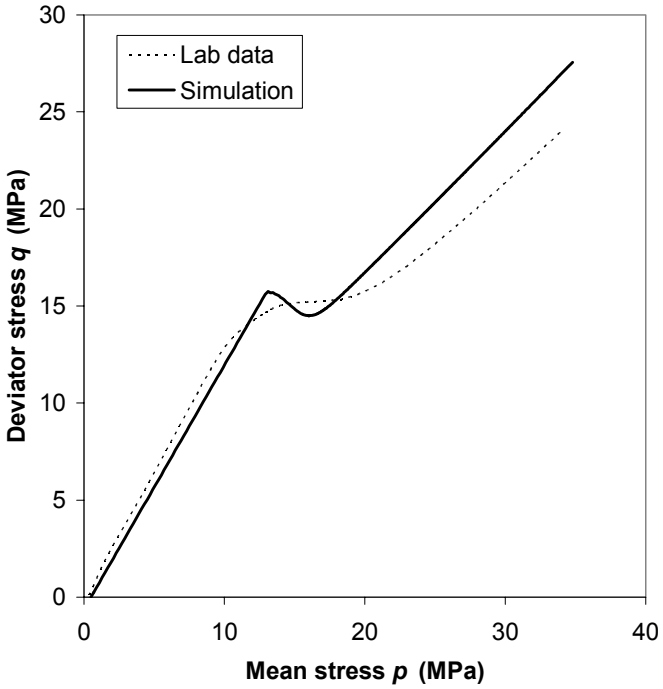

(b)

Figure 8.20. Results of simulated K_0 compression test on oil-saturated Tyra field chalk (File 453). Results include (a) stress-strain curve; and (b) stress path.

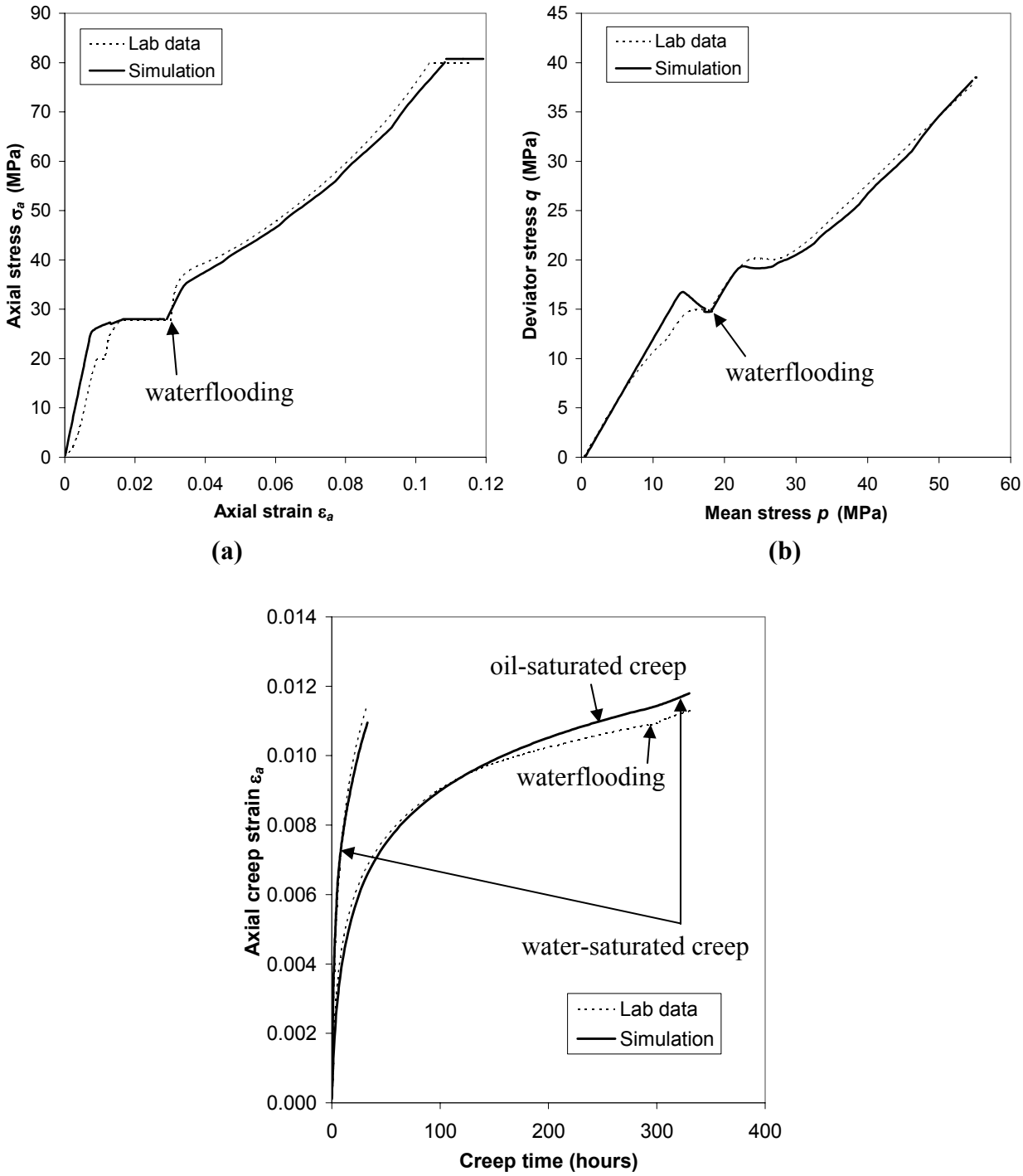

Figure 8.21. Results of simulated waterflooding test on Tyra field chalk (File 454). Results include (a) stress-strain curve; (b) stress path; and (c) creep curves.

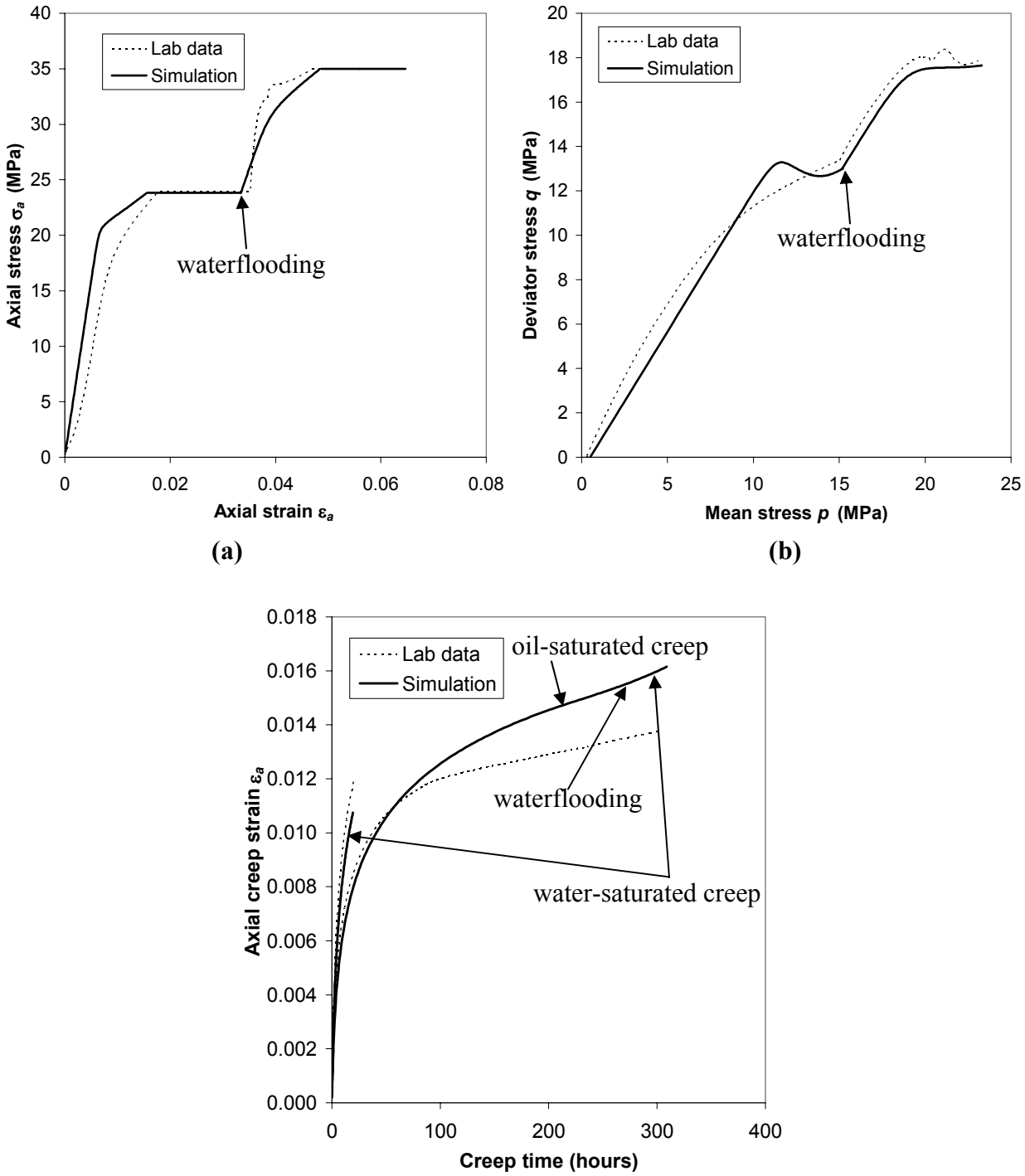

Figure 8.22. Results of simulated waterflooding test on Tyra field chalk (File 455). Results include (a) stress-strain curve; (b) stress path; and (c) creep curves.

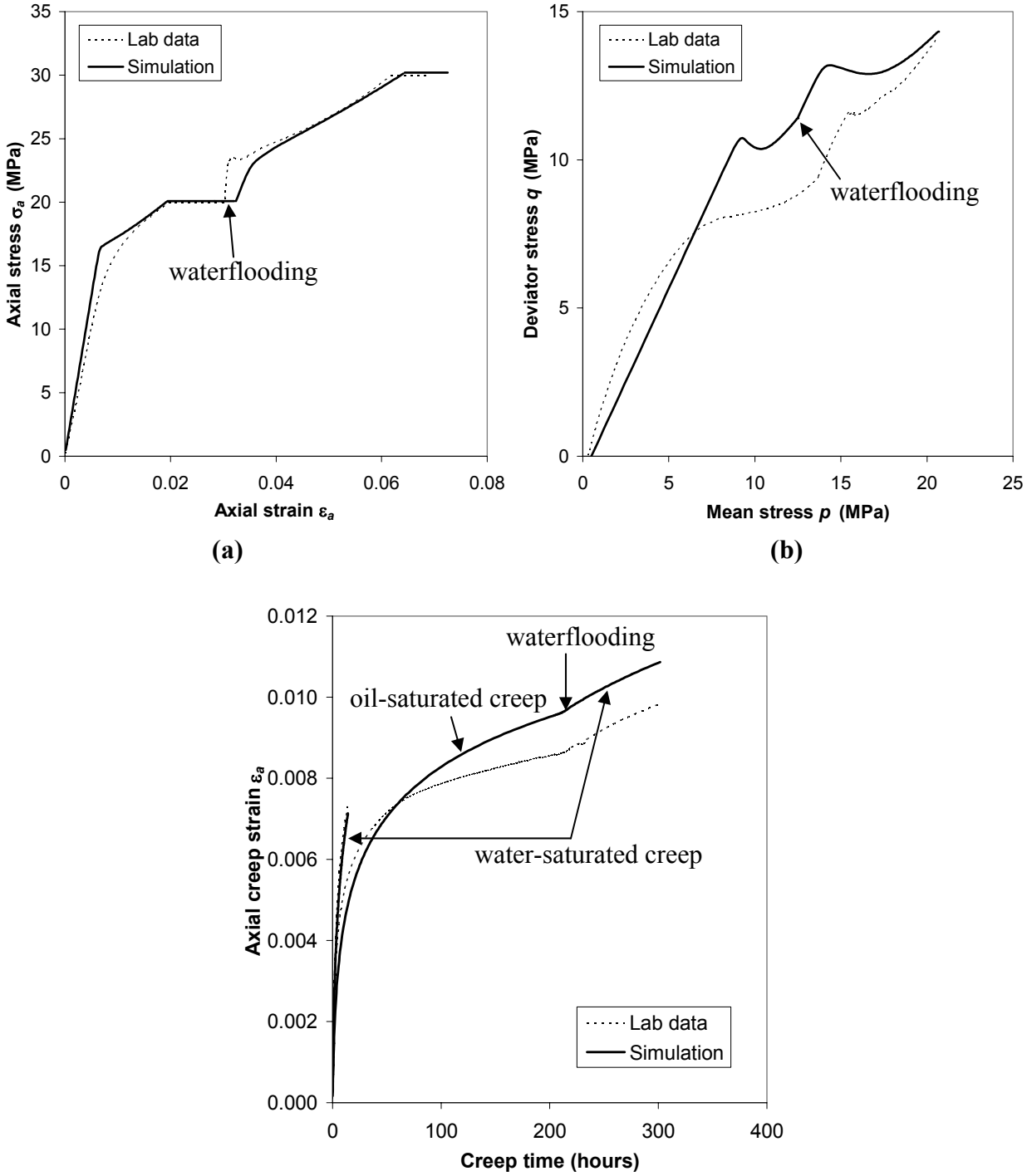

Figure 8.23. Results of simulated waterflooding test on Tyra field chalk (File 456). Results include (a) stress-strain curve; (b) stress path; and (c) creep curves.

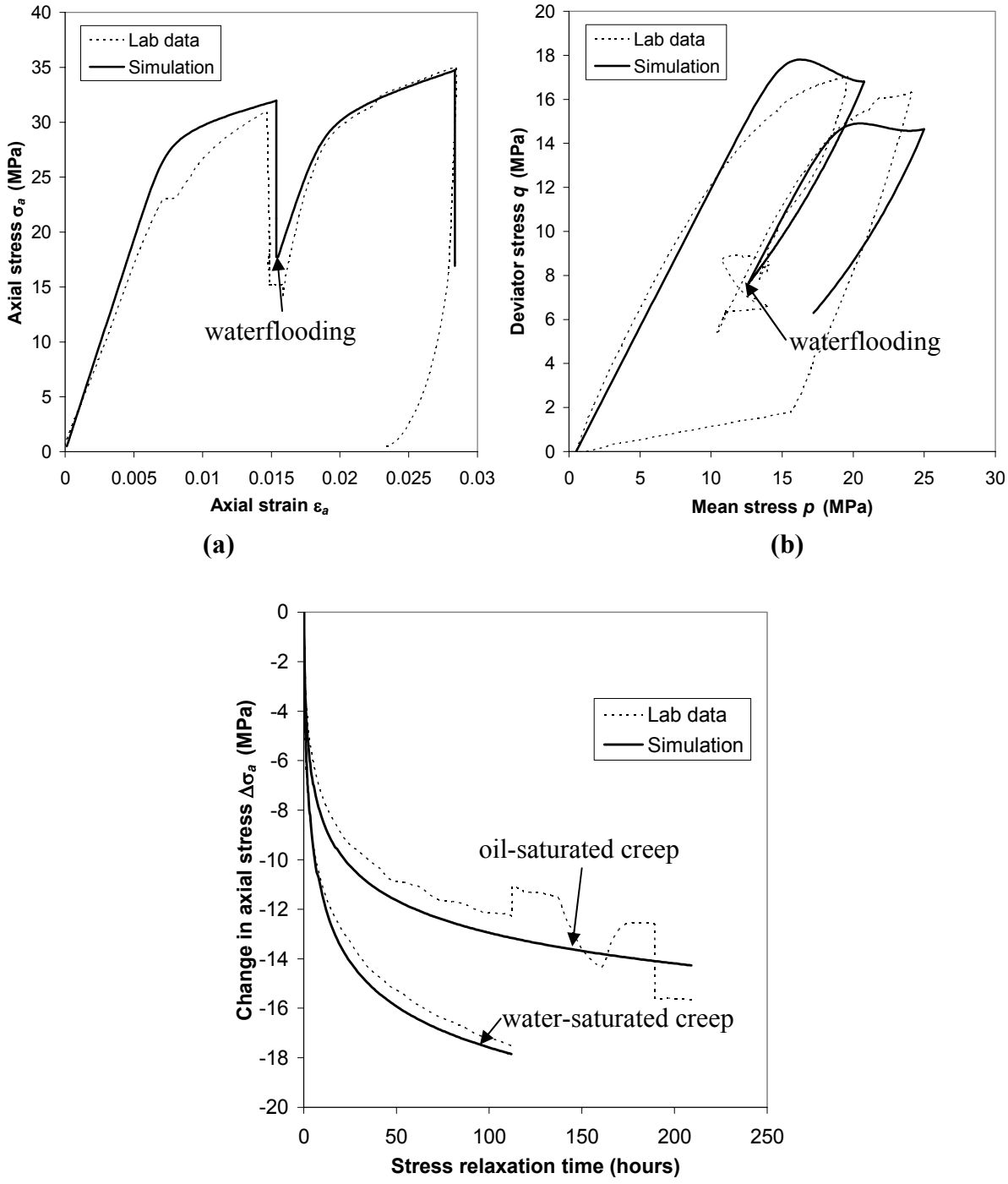

Figure 8.24. Results of simulated waterflooding test on Valhall field chalk (File 500). Results include (a) stress-strain curve; (b) stress path; and (c) stress relaxation curves.